



**HAL**  
open science

# Aerothermal Computations for Laminar–Turbulent Transition Onset Measurement Using Infrared Imaging Technique

Maxime Lalande, Olivier Vermeersch, Fabien Méry, Philippe Reulet, Maxime Forte

► **To cite this version:**

Maxime Lalande, Olivier Vermeersch, Fabien Méry, Philippe Reulet, Maxime Forte. Aerothermal Computations for Laminar–Turbulent Transition Onset Measurement Using Infrared Imaging Technique. *AIAA Journal*, 2022, 61 (1), pp.145-159. 10.2514/1.J062048 . hal-03982940

**HAL Id: hal-03982940**

**<https://hal.science/hal-03982940>**

Submitted on 10 Feb 2023

**HAL** is a multi-disciplinary open access archive for the deposit and dissemination of scientific research documents, whether they are published or not. The documents may come from teaching and research institutions in France or abroad, or from public or private research centers.

L'archive ouverte pluridisciplinaire **HAL**, est destinée au dépôt et à la diffusion de documents scientifiques de niveau recherche, publiés ou non, émanant des établissements d'enseignement et de recherche français ou étrangers, des laboratoires publics ou privés.

# Aerothermal computations for laminar-turbulent transition onset measurement using Infra-Red imaging technique

Maxime Lalande <sup>\*</sup>, Olivier Vermeersch <sup>†</sup> and Fabien Méry <sup>‡</sup>  
*ONERA–The French Aerospace Lab, Université de Toulouse, F-31000 Toulouse, France*

Philippe Reulet <sup>§</sup>  
*ONERA–The French Aerospace Lab, Université de Toulouse, F-31000 Toulouse, France*

Maxime Forte <sup>¶</sup>  
*ONERA–The French Aerospace Lab, Université de Toulouse, F-31000 Toulouse, France*

**This article deals with the computation of heat exchange in transitional boundary layers for the prediction of the laminar-turbulent transition detection using infra-red thermography. An aerothermal coupling between a heat equation solver and a boundary-layer solver is presented here. This coupling is first used to provide guidelines in the academic framework of a flat plate, to achieved an enhanced temperature gradient at the transition onset in order to improve infra-red imaging, and thus the transition position detection. The method is then successfully applied on a real case, by comparing the numerical predictions to measurements obtained during transonic wind-tunnel tests on a two-dimensional wing model.**

## Nomenclature

$T$	=	Temperature K
$T_{ray}$	=	Radiative temperature of the environment K
$T_{aw}$	=	Adiabatic wall temperature, also called friction temperature or recovery temperature $T_{rec}$ K
$T_w$	=	Wall temperature K
$\rho$	=	Density $\text{kg m}^{-3}$
$c_p$	=	Specific heat at constant pressure $\text{J kg}^{-1} \text{K}^{-1}$
$h$	=	Enthalpy $\text{J kg}^{-1}$
$k$	=	Conductivity $\text{W m}^{-1} \text{K}^{-1}$
$Q$	=	Heat volume source term $\text{W m}^{-3}$
$\phi$	=	Heat flux $\text{W m}^{-2}$

---

<sup>\*</sup>Graduate Student, DMPE, maxime.lalande@onera.fr

<sup>†</sup>PhD, DMPE, olivier.vermeersch@onera.fr

<sup>‡</sup>PhD, DMPE, fabien.mery@onera.fr

<sup>§</sup>PhD, DMPE, philippe.reulet@onera.fr

<sup>¶</sup>PhD, DMPE, maxime.forte@onera.fr

$h_f$	= Convective heat transfer coefficient $\text{W m}^{-2} \text{K}^{-1}$
$\epsilon$	= Emissivity
$\sigma$	= Stefan-Boltzmann constant $\text{W m}^{-2} \text{K}^{-4}$ $\sigma = 5.67 \times 10^{-8} \text{W m}^{-2} \text{K}^{-4}$
$M$	= Mach number
$P$	= Pressure Pa
$K_p$	= Pressure coefficient $K_p \stackrel{\text{def}}{=} \frac{P - P_0}{\frac{1}{2}\rho_0 U_0^2}$
$r$	= Recovery factor, for a flat plate $r_{lam} = 0.85$ for laminar flow and $r_{turb} = 0.9$ for turbulent flow
$\gamma$	= Specific heat ratio, for the air $\gamma = 1.4$ in the ideal gas hypothesis validity range
$\mathcal{M}$	= Gas molar mass, for the air $\mathcal{M} = 29 \times 10^{-3} \text{kg mol}^{-1}$ in the non reactive range ( $T < 2500\text{K}$ for $P = 10^5\text{Pa}$ )
$\mathfrak{R}$	= Molar (universal) gas constant $\mathfrak{R} = 8.314 \text{J K}^{-1} \text{mol}^{-1}$
$R$	= Gas specific (or individual) constant, $R \stackrel{\text{def}}{=} \mathfrak{R}/\mathcal{M}$ , for the non reactive air $R = 287 \text{J kg}^{-1} \text{K}^{-1}$
$(x, y, z)$ or $(x_i)$	= Space coordinates m
$(U, V, W)$ or $(U_i)$	= Mean flow velocity components $\text{m s}^{-1}$
$(u, v, w)$ or $(u_i)$	= Local flow velocity components $\text{m s}^{-1}$
$\tau$	= Shear stress Pa
$\mu$	= Dynamic viscosity $\text{kg m}^{-1} \text{s}^{-1}$
$\nu$	= Kinematic viscosity $\text{m}^2 \text{s}^{-1}$
$C_f$	= Skin friction coefficient
$C_h$	= Heat transfer coefficient $C_h \stackrel{\text{def}}{=} h_f / U \rho c_p$ , or Stanton number $St$
$s$	= Reynolds analogy factor $s \stackrel{\text{def}}{=} 2C_h / C_f$ , for a flat plate $s = 1.24$
$\Gamma$	= Intermittency function
$L$	= Reference scale m
$Re_L$	= Reynolds number $Re_L \stackrel{\text{def}}{=} \rho U L / \mu$
$\delta_1$	= Boundary-layer displacement thickness m
$\theta$	= Boundary-layer momentum thickness m
$H$	= Boundary-layer shape factor $H \stackrel{\text{def}}{=} \delta_1 / \theta$
$N$	= Boundary-layer $N$ -factor quantifying the amplification of instabilities
$Fo$	= Fourier number $Fo \stackrel{\text{def}}{=} k \Delta t / \rho c_p L^2$
$Bi$	= Biot number $Bi \stackrel{\text{def}}{=} h_f L / k_m$
$Tu$	= Turbulence rate
$\mathcal{P}$	= Prandtl number $\mathcal{P} \stackrel{\text{def}}{=} \mu c_p / k_f$ , $\mathcal{P} = 0,72$ for the air
$\mathcal{P}_t$	= Turbulent Prandtl number, set to $\mathcal{P}_t = 0,89$

## I. Introduction

THE study of the laminar-turbulent transition of the boundary layer is still currently of great importance, not only to improve our understanding of the destabilizing mechanisms from a fundamental research point of view, but also since it is related to industrial considerations, including increased laminarity. Indeed, it is estimated that for transonic transport aircraft on which the flow can be maintained laminar on a significant part of the wings and other control surfaces (nacelles, horizontal and vertical tail plans), the friction drag could be reduced up to 15% [1]. The design and development of such laminar surfaces require wind tunnel tests and flight experiments during which the transition of the flow from the laminar to the turbulent regime has to be measured and monitored.

Several measurement techniques are used for boundary-layer transition detection beginning with hot-wire (time-resolved velocity measurement)/ hot-film (time resolved skin friction measurement) anemometry. Hot-wire probing was used by Schubauer and Skramstad [2] to first prove the existence of growing perturbations in the laminar region of the boundary layer. Time-resolved local pressure measurements (microphones, kulites, PCB captors ...) can also be used to determine the transition onset characterized by a significant increase of the broadband oscillations in pressure evolution. In the past decades, sublimation techniques, consisting in applying a chemical coating (naphtalene, acenaphtene) on the surface model that sublimate faster in the turbulent region than in the laminar region, were also used to determine transition. This method provides accurate images of the transition line but is less and less employed since it requires steady test conditions. Additionally, the coating needs to be re-applied after each tests, and the chemical reagents usually used may be carcinogens.

Specific sensitive paint (to local shear-stress, pressure and/or temperature) also enable to identify the laminar-turbulent transition region and are interesting measuring devices which experiment a strong development for many years. This is particularly the case for Temperature Sensitive Painting (TSP), which can be used in cryogenic wind tunnels [3].

In parallel to these sensitive paints, even though it has been used for the first time in order to detect transition four decades ago, Infra-Red (IR) imaging has undergone significant developments in the past few years and is more and more employed for transition measurements. Lesant *et al.* [4] provide an overview of infrared thermography techniques applied to wind tunnel testing, and recently, Wolf *et al.* [5] proposed an overview of the IR measurement especially dedicated to boundary layer transition measurement. It is well known that a turbulent boundary layer has greater (5 to 7 times) skin friction coefficient than a laminar one. Moreover, the Reynolds analogy linearly links the skin friction coefficient  $C_f$  to the convective heat transfer coefficient  $C_h$  (also known as the Stanton number  $S_r$ ). As a consequence, the convective heat exchange is lower in the laminar region than in the turbulent one, and the transition is found to be the jump between these two regions and will result in a (large) temperature gradient [4]. By measuring the wall temperature, Infra-Red Thermography (IRT) takes advantage of this phenomenon and if wall temperature difference is large enough, the transition location may be determined. Moreover, IRT is appreciated for being a non-intrusive and global visualization technique that does not require any re-treatment of the model between each test.

The basic principle is to generate a detectable wall temperature difference between the regions of laminar and turbulent flow. This difference is imposed by the convective heat exchange  $\phi = h_f(T_w - T_{aw})$  and will be all the more important when values of the convective heat coefficient  $h_f \propto C_f M_e$  and  $T_{aw} = T_e(1 + 0.2rM_e^2)$  are far from each other depending on the laminar or turbulent state of the flow. Due to the turbulent spots downstream of the transition onset, the skin friction coefficient  $C_f$  and the recovery factor  $r$  increase compared to their value in the laminar conditions. This increase will be greater for larger Mach numbers. This results in a laminar-turbulent difference for  $h_f$  and  $T_{aw}$ , which is all the greater as the Mach number is large. This explains why IR thermography was used first for high speed flow; the first experimental investigations being attributed to Thomann and Frisk [6] in 1968 who measured heat transfer on a paraboloid at Mach 7 in a hypersonic wind tunnel.

Concerning IR imaging applied to study laminar-turbulent transition, the first experimental measurements were conducted by Boucharly and Durand [7] in 1983 for subsonic and transonic flows; due to reduced velocity and since no specific process was set-up to enhance temperature difference between zone exposed to laminar or turbulent flow, the visualisations were hard to read. According to Quast [8] in 1987, a wall temperature difference of the order of the degree between the laminar and the turbulent zones is sufficient to obtain good measurements. In the existing literature, several methods have been investigated in order to enhance this wall temperature difference in particular for the subsonic and transonic regimes. For wind tunnel tests, Quast recommends to switch on/off the wind tunnel cooling system in order to create a thermal disequilibrium between the model and the fluid. For free-flight tests, this can be done by changing aircraft speed and/or altitude. Indeed, in 2000, Banks *et al.* [9] conducted supersonic flight tests and noticed that during return to subsonic speed the wing was still hot enough so that they could have carried out subsonic IR measurements. This technique was employed by Crawford *et al.* [10] to conduct transition measurements during a subsonic flight test. In the same idea, Zuccher and Saric [11] spread liquid nitrogen on the model surface in order to cool it before each testing, even though the cooling effect is temporary and it requires successive applications. One can also use IR lamp to heat the outer surface of the model. This enables to maintain a heat flux over time, but can lead to reflections on the surface (Quast [8]). To prevent this, materials with very high emissivity are used (*e.g.* carbon fiber composite for Raffel and Merz [12]), or an anti-reflective additional layer of high emissivity is added to the surface model (Simon *et al.* [13], Gardner *et al.* [14]). Probably the most used method consists to heat the model on the inner surface by heating wires, as first recommended by Quast. Joseph *et al.* [15] used an aluminium model within which they attached silicone rubber heater. In spite of the non-homogeneous installation of the heaters, the high conductivity of the aluminium permits to obtain an homogeneous distribution of temperature in the model. In order to regulate the heat flux at the external surface, they added an external insulated layer of 800  $\mu\text{m}$  as well as a thin layer of high emissivity and dull paper to prevent from IR reflections. Crawford *et al.* [10] only applied a single high emissivity insulated paint layer of 300  $\mu\text{m}$  on the surface to regulate the flux and prevent the reflections. They also added an insulated layer under the heaters on the internal surface, so as to direct all heat flux to the outer surface. Similar design were used by Simon *et al.* [13] to

perform dynamic detection. Banks *et al.* [9] showed that the thicker the insulation layer, the stronger the temperature gradients, and therefore the easier it is to detect the transition; nonetheless, the use of an insulated layer and its thickness are limited by structural constraints.

Raffel and Merz [12] introduced Differential Infra-red Thermography (DIT), which consists in subtracting two consecutive thermography measurements for a moving model. If the time step between the two IR images is short enough, the final model position will differ very slightly from the initial one corresponding to different but very close conditions in terms of Reynolds and Stanton numbers. This means that the temperature distribution will be different for the two successive positions in particular in the transition region and that the difference between the two images give information on either the beginning and the end of the transition.

Once the temperature field is experimentally measured using IR thermography and some data reduction process, the transition location needs to be determined with the help of a given criterion. The transition onset location can be defined as the highest chordwise temperature gradient [15] or the middle of the intermittency area [14]. This position is roughly constant spanwise for natural transition triggered by Tollmien-Schlichting waves (zero sweep wing), however if one wants to capture a global transition location chordwise for a swept-wing presenting cross-flow vortices, Crawford *et al.* [16] proposed to take the maximum of the Cumulative Distribution Function (CDF), that quantifies the ratio of points being turbulent over a spanwise section.

In practice, the above-mentioned methods used to improve the quality of IR measurements by increasing the temperature gradient at the transition have been developed empirically, and only a few studies have focused on a numerical investigation of the influence of these techniques. Joseph *et al.* [15] have numerically studied the effect of internal heating on the wall temperature evolution with a simple model based on the electrical analogy. The authors also neglected radiation exchanges and the intermittency area of the transition. Gardner *et al.* [14] investigated the time evolution of the temperature profile by coupling a Unsteady Reynolds Averaged Navier Stokes equations (URANS) code and a 1D finite difference thermal scheme (in wall normal direction), but radiation exchanges were also neglected. A more complete modelling that takes every known sources of heat exchange terms into account has been proposed by Banks *et al.* [9] to predict the temperature distribution in a wing in supersonic free-flight conditions. The boundary layer is solved using the so-called integral method, based on closure semi-empirical formulas, and the transition onset location is imposed by the authors.

In turbomachinery, the heat transfer imposed by hot gas is of paramount importance for the design of turbine blades and vanes in particular their cooling systems and/or coatings. This requires numerical tools to accurately predict heat transfer. This problem has been addressed by a so-called Conjugate Heat Transfer (CHT) analysis based on the coupling of a convective fluid solver with a thermal conduction solver in the solid. In practice, each set of equations is solved separately to provide a boundary condition for the other. The two sets of equations are solved in turn until continuity of temperature and heat flux is achieved at the interface. In 2001, Verdicchio *et al.* [17] analyzed the coupling between

a RANS fluid solver and a solid solver for turbine discs. They highlighted out the key role of boundary condition relationships at the interface using two different conditions. The fluid solver was used to specified either heat flux (Neumann boundary condition) or thermal coefficient and fluid temperature (Robin) as boundary condition for the solid solver which propagated back the wall temperature (Dirichlet) to the fluid solver. They emphasized the need of under relaxation of boundary condition values to ensure numerical convergence. Heidmann *et al.* [18] developed a conjugate heat transfer coupling between a RANS solver and a boundary element method solver in order to study heat transfer on a film-cooled vane. The advantage of the boundary element method is that only a surface grid is required to solve the steady conduction problem in the solid. The numerical convergence was achieved using a Temperature Forward Flux Back (also referred as Dirichlet/Neumann) coupling. The flow solver calculates the wall temperature which is specified as a Dirichlet boundary condition to the solid solver. Conduction heat equation is then solved and the solution is sent back to the fluid solver and used as a Neumann thermal boundary condition at the wall. In 2006, Verstrack *et al.* [19] compared Temperature Forward Flux Back (Dirichlet/Neumann) and Flux Forward Temperature Back (Neumann/Dirichlet) coupling strategies to simulate two turbomachinery applications. They also developed a Robin/Dirichlet approach (as proposed by Verdicchio *et al.* [17]) with a predetermined heat transfer coefficient. This last formulation provided faster convergence and more numerical stability than the two previous one. In the same way, Radenac [20] analysed the behaviour of a Neumann/Dirichlet and Robin/Dirichlet coupling between two domains at thermal equilibrium for a one dimension problem. Introducing a temperature disturbance at the vicinity of the interface, he analysed the stability of the boundary condition looking at the evolution of the eigen-values of the problem and demonstrated the unconditional behaviour of the Robin condition compared to the Neumann one. These examples of conjugate heat transfer method demonstrate that the boundary conditions at the interface play a major role in the numerical convergence and the performance of the simulation. They were all performed considering a fully turbulent flow and using a RANS fluid solver. This requires a fine mesh at the wall to accurately capture temperature gradient leading to an important computational cost. The steady fluid state solution is sought by a marching in time until variables reach converged values so that intermediate temporal solutions are not physically meaningful. Additionally, the solid is made of a unique material with a significant conduction coefficient corresponding to small Biot number which makes easier the convergence of the fluid solid coupling. The present work aims at providing a reliable numerical tool able to predict the temperature variations (both in time and in space) of a multi-layer structure. The solid could be made of a low conductivity material and subjected to a transition flow leading to a significant evolution of the convective heat transfer coefficient. Moreover, all thermal effects (conduction, convection and radiation) must be taken into account. This approach is quite similar to the conjugate heat transfer method develop for turbomachinery except that the RANS solver is replaced by a boundary-layer solver. The boundary layer solver allows to improve the computation of fluid properties (temperature gradient, laminar turbulent transition, ...) in the vicinity of the wall with a much lower computational cost. Nevertheless, it requires not only the geometry of the solid but also the external velocity distribution at the edge of the

boundary layer. The latter can be obtained from measurements or low fidelity (potential flow, Euler) computations. However, the curvature of the wall is neglected and the computation is limited to attached flows. The objective of this numerical tool is to provide temperature distribution at the solid surface in order to pre-dimension models and heating devices for measurement of the laminar to turbulent transition by IR imaging, in particular for subsonic and transonic regimes for which the heat exchanges are weak.

First, the coupling method, in particular the boundary conditions between the fluid solver and the heat equation solver in the solid is presented and discussed. A parametric study is then conducted on the academic flat plate case so as to give some guidelines for future experimental tests. This method is then applied on a two-dimensional laminar wing operating in transonic conditions. Numerical predictions are compared with IR measurements performed during a wind tunnel test campaign in 2021.

## II. Equations and numerical solvers

In order to take into account the thermal effects in the model and the boundary-layer behavior as well, two ONERA in-house codes have been coupled. This section aims at introducing these solvers and the associated equations.

### A. Heat equation in the solid

One considers a model upon which a transitional boundary layer is developing, see Fig. 1.

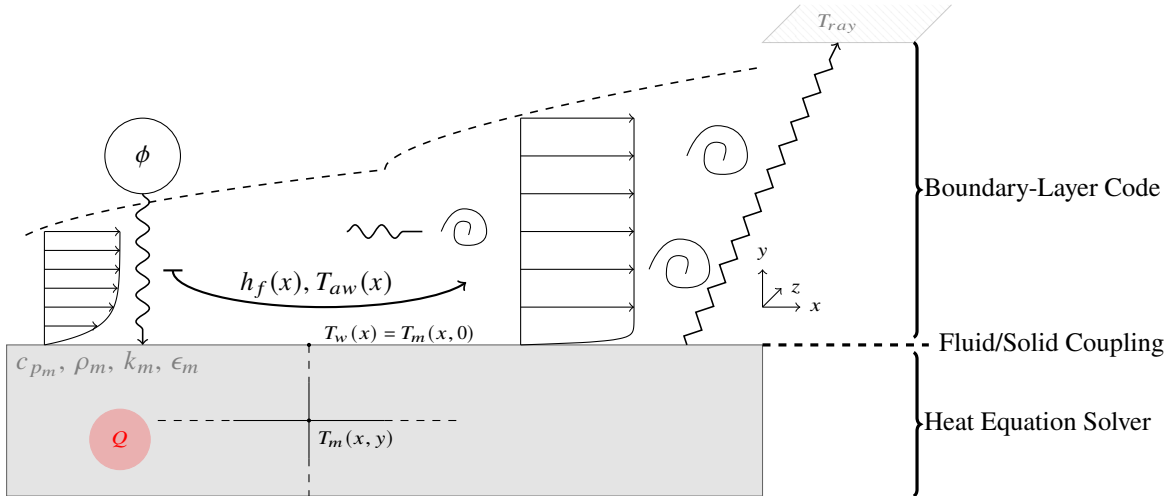


Fig. 1 Sketch of heat transfer on a model

The heat transfer equation inside the material is given by:

$$\rho_m c_{p_m} \frac{\partial T_m}{\partial t} - \nabla \cdot (k_m \nabla T_m) = Q \quad (1)$$

where  $T_m$  is the temperature inside the material,  $\rho_m$  is the density of the material,  $c_{p_m}$  its heat capacity at constant

pressure and  $k_m$  its thermal conductivity.  $Q$  is a volume production term.

The boundary condition on the external surface on which the boundary-layer flow is developing is given by:

$$k_m \left( \frac{\partial T_m(x, y)}{\partial y} \right)_{y=0} = \phi + h_f(x) (T_{aw}(x) - T_w(x)) + \epsilon \sigma (T_{ray}^4 - T_w^4(x)) \quad (2)$$

where  $h_f$  is the (convective) heat transfer coefficient imposed by the boundary-layer flow. The adiabatic wall temperature  $T_{aw}$  stands for the temperature of the wall in adiabatic conditions *i.e.* without any heat transfer between the flow and the material. This temperature is also called friction temperature or recovery temperature  $T_{rec}$  since it would be the temperature reached by the wall if the model was exposed for a long time to a given flow. Both the convective heat transfer coefficient and the adiabatic wall temperature depend on the laminar or turbulent state of the boundary layer. The emissivity of the material  $\epsilon$  ranges from 0 to 1 (maximum value corresponding to a black body). For a metallic polished wall  $\epsilon \approx 0.1$ , while when black painted the emissivity increases up to  $\epsilon \approx 0.9$ . The constant  $\sigma = 5.67 \times 10^{-8} \text{W m}^{-2} \text{K}^{-4}$  is the Stefan-Boltzmann constant and  $T_{ray}$  the radiative temperature of the environment\*.

An in-house code [21, 22] solving this set of equations for a multi-layer material is used. The spatial resolution is based on a finite volume formulation, with a regular and structured mesh. The time discretization is performed by the  $\theta$ -method. For an ordinary differential equation (ODE)  $u' = g(u)$ , the time discretisation of the  $\theta$ -method takes the form:  $u_j = u_{j-1} + \Delta t(1 - \theta)g(u_{j-1}) + \Delta t\theta g(u_j)$ . The Backward Euler method (*i.e.*  $\theta = 1$ ) is used for a stationary desired state, and the Crank-Nicolson method (*i.e.*  $\theta = 1/2$ ) for an unsteady calculation. In both cases, the schemes are stable for every Fourier number  $Fo = \frac{k\Delta t}{\rho C_p L^2}$ , even though a too large  $Fo$  leads to numerical oscillations for  $\theta = 1/2$ . On the contrary, a too low  $Fo$  results in slow convergence. Hence, it is recommended to have  $Fo \approx 0.5$  when using the Crank-Nicolson integration scheme.

## B. Fluid boundary-layer equations

### 1. Prandtl equations for the mean flow

For a two-dimensional, steady, compressible boundary-layer flow, the Navier-Stokes equations are reduced to the following set of equations (3), known as the boundary-layer or Prandtl equations:

$$\begin{cases} \frac{\partial \rho u}{\partial x} + \frac{\partial \rho v}{\partial y} = 0 \\ \rho u \frac{\partial u}{\partial x} + \rho v \frac{\partial u}{\partial y} = \rho_e U_e \frac{dU_e}{dx} + \frac{\partial \tau}{\partial y} \\ \rho u \frac{\partial h_i}{\partial x} + \rho v \frac{\partial h_i}{\partial y} = \frac{\partial (u\tau - \phi)}{\partial y} \end{cases} \quad (3)$$

In the momentum equation (second equation of the system), the viscous stress  $\tau$  depends on the regime of the

---

\*For wind-tunnel test, this reference temperature stands for the test section wall temperature,  $T_{ray} \approx T_i$ . For a flight test, it corresponds to the temperature of the sky  $T_{ray} \approx 0\text{K}$ .

boundary layer , see Eq. (4). Using the Reynolds decomposition of the flow quantities into a mean value and a fluctuation part  $\tilde{q} = q + q'$ , with respect to a given average function  $\langle . \rangle$  such that  $\langle \tilde{q} \rangle = q$ :

$$\begin{cases} \tau_{\text{lam}} = \mu \frac{\partial u}{\partial y} \\ \tau_{\text{turb}} = \mu \frac{\partial u}{\partial y} - \rho \langle u'v' \rangle \end{cases} \quad (4)$$

In the energy equation (third equation of the system (3)),  $h_i = h + |\vec{u}|^2 / 2$  the total enthalpy, and  $\phi$  the heat flux, also depend on the flow regime , see Eq. (5):

$$\begin{cases} \phi_{\text{lam}} = -k \frac{\partial T}{\partial y} \\ \phi_{\text{turb}} = -k \frac{\partial T}{\partial y} + \rho \langle v'h' \rangle \end{cases} \quad (5)$$

The perfect gas law (6) closes the equation system for a compressible gas:

$$P = \rho \frac{\mathfrak{R}}{\mathcal{M}} T = \rho RT \quad (6)$$

In the present study, the turbulence stress  $\langle u'v' \rangle$  is modeled using the Boussinesq hypothesis through a turbulent viscosity (also referred as eddy viscosity)  $\mu_t$ :

$$-\rho \langle u'v' \rangle = \mu_t \frac{\partial u}{\partial y} \quad (7)$$

This eddy viscosity is expressed by an algebraic model (sometimes referred as the '0-equation' or '0-order' model) using the concept of mixing length turbulence model  $l$  such as:

$$\mu_t = \rho l^2 \frac{\partial u}{\partial y} \quad (8)$$

In the logarithmic region, the variation of the eddy viscosity is imposed by inertial turbulent stress so that the viscous stress can be neglected. It can be therefore shown that theoretically the mixing length depends linearly on the wall distance  $l = \chi y$ , with  $\chi = 0.41$  the von Kàrmàn constant. In the external region, turbulence length scale  $l$  is related to the boundary-layer thickness  $\delta$  and experiments [23] have shown that the ratio  $l/\delta$  becomes constant close to 0.085. In 1969, Michel [24] proposed an analytical formulation for the mixing length verifying a linear behavior for small wall distance ( $l = \chi y$ ) and reaching a constant value of 0.085 towards the outer edge of the boundary layer:

$$\frac{l}{\delta} = 0.085 \tanh \left( \frac{\chi}{0.085} \frac{y}{\delta} \right) \quad (9)$$

Nonetheless, the expression (9) is only valide in fully turbulent zone where inertial stress is prevailing. Close to the wall, viscous damping has to be taken into account. This effect is represented by a corrective function  $F$  that ensures the appropriated damping of velocity fluctuations moving towards the wall so that the viscous diffusion ( $\nu$ ) becomes dominating compared to the turbulent one, see Eq. (10):

$$F = 1 - \exp\left(-\frac{l}{26\chi\mu} (\tau\rho)^{1/2}\right) \quad (10)$$

Finally, turbulent stress and turbulent heat flux are given by:

$$\begin{cases} -\rho \langle u'v' \rangle = \rho \left( (Fl)^2 \frac{\partial u}{\partial y} \right) \frac{\partial u}{\partial y} = \mu_t \frac{\partial u}{\partial y} \\ -\rho \langle v'h' \rangle = -\rho \left( \frac{1}{\mathcal{P}_t} (Fl)^2 \frac{\partial u}{\partial y} \right) \frac{\partial h}{\partial y} = -\left( \frac{\mu_t}{\mathcal{P}_t} \right) \frac{\partial h}{\partial y} = -k_t \frac{\partial h}{\partial y} \end{cases} \quad (11)$$

where  $\mathcal{P}_t$  is the turbulent Prandtl number set to a constant value  $\mathcal{P}_t = 0.89$ .

The mixing length turbulence model suffers from the same restrictions as the boundary-layer solver neglecting wall curvature and is not adapted to represent vortex regions such as separation regions. Moreover, it is restricted to moderated external pressure gradient, low external turbulence level and does not account for wall roughness effect. Such limitation could be raised by the use of more elaborated turbulence models such as 2<sup>nd</sup>-order formulations (*e.g.*  $k - \epsilon$  or  $k - \omega$  turbulence models). It has been verified, both for the flat plate (section IV Guidelines for IR measurements) and for the transonic airfoil (section V Application on real cases), on some configurations that the mixing length approach provided results close to the one obtained with the  $k - \epsilon$  [25] and a  $k - \omega$  [26] models.

The boundary-layer Prandtl equations are parabolic in nature, so that they can be solved employing a streamwise marching procedure [27]. The computation is initialized at the first point by a self similar analytical velocity profile: either the Blasius profile for the flat plate case or the Hiemenz velocity profile (stagnation point) for a 2D airfoil configuration. The space step is automatically adjusted in order to have the best progression between two consecutive points.

## 2. Modelling of the transitional region

The boundary-layer solver [27] performs a simplified modeling of the linear stability calculation to compute the boundary-layer  $N$ -factor, using the parabolus method first introduced by Arnal [28] which gives an approximated value of the amplification rate as a function of the shape factor  $H$  and the local Reynolds number  $Re_{\delta_1}$  based on the boundary-layer displacement thickness. More details about this transition prediction method can be found in [29]. The streamwise integration of these amplification rates provides the value of the so-called  $N$ -factor which can be interpreted as the spatial amplification of a physical boundary-layer instabilities.

The  $e^N$  criterion is used, which means that transition occurs when the  $N$ -factor exceed a given limit  $N_T$ , that is for TS induced transition related to the turbulence rate of the external flow by the Mack relation [30]:

$$N_T = -8.43 - 2.4 \ln Tu, \quad 1 \times 10^{-3} < Tu < 1 \times 10^{-2} \quad (12)$$

Once the starting point of the transition is specified by the  $e^N$  criterion, the boundary layer develops from a laminar to a turbulent state characterized by a change in its properties. In particular, the turbulent contributions ( $\mu_t$  and  $k_t$ , see equation (11)) are added to the natural viscosity and conductivity of the fluid to model the impact of turbulent spots on the mean-flow. An intermittency function, quoted  $\Gamma$ , is used to smooth the evolution of the effective viscosity from laminar to turbulent state:

$$\mu_{eff} = \mu + \Gamma \mu_t \quad (13)$$

In the present study,  $\Gamma$  is the intermittency function of Dhawan and Narasimha [31]:

$$\Gamma(x) = 1 - \exp\left(-0.412 \left(\frac{x - x_T}{\lambda_T}\right)^2\right) \quad (14)$$

With  $x_T$  the transition position and  $\lambda_T$  a parameter related to the extend of the transitional region that can be related to  $\Delta x = x_{\Gamma=0.999} - x_T = 4.1\lambda_T$ . According to Stock and Haase [32],  $\Delta x$  and the displacement thickness at the transition  $\delta_{1,T}$  are related by the relationship  $Re_{\Delta x} = 13.4Re_{\delta_{1,T}}^{3/2}$  which allows to express the extend parameter  $\lambda_T$  as a function of the displacement thickness at the transition onset.

$$Re_{\Delta x} = 13.4Re_{\delta_{1,T}}^{3/2} \quad (15)$$

In the same way, the intermittency function is involved in the expression of the adiabatic wall temperature which is given by the relation:

$$T_{aw} = T_i \frac{1 + r \frac{\gamma-1}{2} M_e^2}{1 + \frac{\gamma-1}{2} M_e^2} \quad (16)$$

With  $r$  the recovery factor, constant and dependant of the flow regime:  $r^{lam} = 0.85$  and  $r^{turb} = 0.90$ . To avoid any discontinuity in the streamwise evolution of  $T_{aw}(x)$  at the transition onset, the intermittency function is used to weight the evolution of the recovery factor in the transitional zone such as:

$$r = (1 - \Gamma)r^{lam} + \Gamma r^{turb} \quad (17)$$

### III. Aerothermal coupling condition

#### A. Different ways of coupling and convergence

**Different ways of coupling** Several strategies exist to realize an aero (fluid)/thermal (solid) coupling. Here we focus on a partitioned approach: the fluid and solid equations are solved separately and the coupling between the fluid and solid solvers is done by treating the boundary conditions imposed on the two domains. To achieve this coupling, it is necessary to ensure the equality of the temperature and heat flux at the interface. To guarantee the temperature equality, the wall temperature is computed by the solid solver and directly imposed on the fluid domain at the interface. This corresponds to a Dirichlet type boundary condition. Concerning the heat flux, two kind of boundary conditions can then be used:

- The heat flux  $\phi_w$ , computed by the fluid solver, can be directly imposed on the interface of the solid. This is a Neumann type boundary condition which implies that during the whole resolution of the solid solver  $\phi_w$  remains constant and is not influenced by the evolution of  $T_w$ . The flux is therefore *only* updated at the next call of the fluid solver. It is easy to understand that  $T_w$  must not evolve much between two cycles of the coupling or it might lead to convergence issues.
- A convection model  $\phi_w = h_f(T_{aw} - T_w)$  can be used and is usually referred as Robin (or Fourier) type boundary condition. The convective heat exchange coefficient  $h_f$  and the adiabatic wall temperature  $T_{aw}$  are computed by the fluid solver. The value of the flux is thus adapted at each computational iteration of the solid solver with the evolution of  $T_w$ .

**Numerical stability** A large number of works focus on the study of the stability of partitioned aerothermal couplings depending on the type of boundary conditions chosen. In this study, we have considered both a Neumann/Dirichlet and a Robin/Dirichlet coupling:

- Neumann/Dirichlet: Radenac [20] indicates that the stability is conditioned by the ratio of the conductivities of the fluid and solid domains: it is then necessary to have the conductivity of the fluid lower than the conductivity of the solid:  $k_f < k_m$ . Moreover, Verstraete [33] showed that the Biot number must verify  $Bi < 1$ , with  $Bi = hL/k = t_{\text{conduction}}/t_{\text{convection}}$ . This shows that on the one hand, the convective resistance must be greater than the conductive resistance, which is consistent with Radenac's criterion:  $1/k_f > 1/k_m$ . On the other hand, it indicates that the characteristic time of conduction must be lower than that of convection. In other words, conduction must not be allowed to take place too much between two updates of the flow, *i.e.*  $T_w$  must not evolve too much between two calls of the fluid solver.
- Robin/Dirichlet: Radenac [20] has shown that such a coupling is theoretically unconditionally stable.

## B. Neumann/Dirichlet Coupling

In a Neumann/Dirichlet coupling, the temperature equality is ensured by a Dirichlet condition on the fluid domain from the wall temperature  $T_w$  calculated by the solid solver. The continuity of the heat flow is ensured by a Neumann condition where  $\phi_w$  is computed by the fluid solver and imposed on the solid domain in addition to the contribution of the radiation and of a hypothetical external flux (external heating by an IR lamp for example):

$$k_m \left( \frac{\partial T_m(x, y)}{\partial y} \right)_{y=0} = \phi_w + \phi_{ext} + \epsilon \sigma \left( T_{ray}^4 - T_w^4(x) \right) \quad (18)$$

Where  $\phi_w$  is computed by the fluid solver from the enthalpy:

$$\phi_w = k_f \left. \frac{dT}{dy} \right|_{y=0} = \frac{\mu c_p}{\mathcal{P}} \left. \frac{dT}{dy} \right|_{y=0} = \frac{\mu}{\mathcal{P}} \left. \frac{dh}{dy} \right|_{y=0} \quad (19)$$

The coupling is initialized with a uniform temperature field in the solid (fluid stagnation temperature  $T_i$  for instance). At each calling of the boundary-layer code, the wall temperature is extracted and imposed on the fluid domain boundary. The boundary-layer code solves the compressible Prandtl equations with an anisothermal wall and computes the heat flux at the wall. This flux is used as the boundary condition of the solid solver. The latter solves the unsteady heat equation over a time period  $n_t \Delta t$ , with  $n_t$  the number of time iterations and  $\Delta t$  the time step (Backward Euler scheme). As mentioned before,  $T_w$  must not evolve too much between two calls of the fluid solver, in other words  $n_t \Delta t < t_{cara}$  to ensure stability. This characteristic time depends strongly on the value of  $\tilde{Bi} = \tilde{h}_f e / k_m$ , with  $\tilde{h}_f = \max_x(h_f)$ . For example, for a flat plate covered with a  $e = 2\text{mm}$  insulator of conductivity  $k_m$  on which a transitional boundary layer develops at  $M = 0.8$  ( $\tilde{h}_f \approx 400\text{W m}^{-2} \text{K}^{-1}$ ), we find:

- $k_m = 0.05\text{W K}^{-1} \text{m}^{-1}$ :  $\tilde{Bi} = 16$ , the calculation never converges regardless of how small is  $n_t \Delta t$
- $k_m = 0.5\text{W K}^{-1} \text{m}^{-1}$ :  $\tilde{Bi} = 1.6$ , the calculation converges for  $n_t \Delta t < 1\text{s}$
- $k_m = 5\text{W K}^{-1} \text{m}^{-1}$ :  $\tilde{Bi} = 0.16$ , the calculation converges for  $n_t \Delta t < 240\text{s}$

Convergence is very slow for a  $Bi$  number close to unity, and rather fast for  $Bi < 1$ , which is consistent with the Verstraete's condition. We decided to impose  $n_t = 50$  as a constant, then to adapt  $\Delta t$  accordingly to ensure  $n_t \Delta t < t_{cara}$ . Even if an explicit relation between  $Bi$  and  $t_{cara}$  could not be exhibited, as other parameters also have an influence on the stability, several tests have shown that setting  $\Delta t = 0.02$  for  $Bi > 0.05$  and  $\Delta t = 5$  for  $Bi < 0.05$  allowed for a stable coupling. After each calling of the fluid solver,  $\tilde{Bi}$  is calculated from  $\tilde{h}_f$ . For this, we use the Reynolds analogy which links the friction coefficient  $C_f$  calculated by the fluid solver to  $h_f$ :

$$C_h \stackrel{\text{def}}{=} \frac{h_f}{\rho c_p U_e} \stackrel{\text{analogy}}{\equiv} \frac{s}{2} C_f \quad (20)$$

with the analogy factor set to  $s = \mathcal{P}^{-2/3} = 1.24$ , and  $U_e$  the velocity at the outer boundary-layer edge.

In practice, we consider cases with very low material surface conductivities (using of insulators to improve IR measurements), which implies a high Biot number, and therefore  $n_r \Delta t$  too low. The algorithm multiplies the cycles between the fluid and solid solver, which makes the computation time increase.

### C. Robin/Dirichlet coupling method

In a Robin/Dirichlet coupling the continuity of the heat flux with the fluid at the solid interface is ensured by a convection model:

$$k_m \left( \frac{\partial T_m(x, y)}{\partial y} \right)_{y=0} = \phi_{ext} + h_f(x) (T_{aw}(x) - T_w(x)) + \epsilon \sigma (T_{ray}^4 - T_w^4(x)) \quad (21)$$

The convective heat exchange coefficient  $h_f$  can be obtained directly from the heat flux at the wall calculated by the fluid solver:

$$h_f = \frac{-\frac{\mu}{\mathcal{P}} \frac{\partial h}{\partial y} \Big|_{y=0}}{T_w - T_{aw}} \quad (22)$$

The adiabatic wall temperature is given by equations (16) and (17).

However, in some cases the wall temperature  $T_w$  may gets too close to the adiabatic wall value  $T_{aw}$ , which results in a  $h_f$  tending to infinity. This may appear when other heat sources (external flux, radiation, internal heating) than the fluid itself are weak which may be the case for wind tunnel tests. In that situation, the convective term becomes predominant in the boundary condition equation, so  $T_w$  gets even closer to  $T_{aw}$ , and so on, which makes the calculation diverge.

The convective heat exchange coefficient  $h_f$  must therefore be calculated differently to avoid any divergence when the wall temperature tends toward its adiabatic value  $T_w \rightarrow T_{aw}$ . One possibility is to use the Reynolds analogy (20) which assumes a direct proportionality between the heat transfer and the skin friction coefficients.

Theoretically, such a coupling is unconditionally stable [20] and one does not need to pay attention to the Biot number  $Bi$  or any other stability criterion. The temperature in the solid is initialized to  $T_i$ . The boundary-layer code solves the Prandtl equations and returns the skin friction coefficient  $C_f$  and the adiabatic wall temperature  $T_{aw}$ . The convective heat exchange coefficient  $h_f$  is calculated from  $C_f$  using the Reynolds analogy and the distribution of  $h_f$  and  $T_{aw}$  on the edge of the solid domain is imposed. The solid solver resolves the heat equation to reach a steady state. The surface temperature is extracted and fed back to the fluid solver as a Dirichlet condition. This process is performed until the surface temperature converges, which usually takes no more than 5 cycles. The figure 2 pictures this iterative process.

This coupling has the advantage of not being limited by the conductivity of the material, and always converges in a

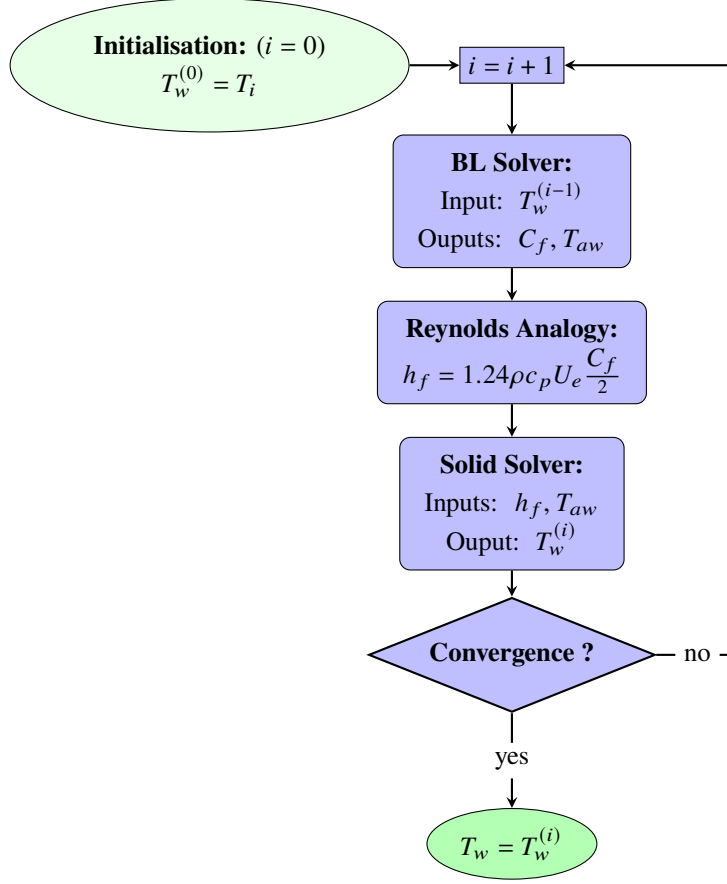


**Fig. 2 Iterative process of the Robin/Dirichlet coupling method**

few minutes. On the other hand, the Neumann/Dirichlet coupling requires several hours to converge for an insulator of very low conductivity.

The comparison of the wall temperature is plotted for two Mach numbers in figure 3. The flow develops along a flat plate consisting of a 20 mm aluminium layer covered with a 2 mm epoxy insulator of conductivity  $k = 0.5 \text{ WK}^{-1} \text{ m}^{-1}$  on which a transitional boundary layer develops. The  $e^N$  approach based on the Arnal parabola method is used to calculate the position of the transition onset with a N-factor before the destabilization of the boundary layer by Tollmien-Schlichting waves is taken at  $N_{\text{TS}} = 6$ .

The differences between the temperatures calculated by these two couplings on the considered cases are rather small compared to the wall temperature difference  $\Delta T$  between the laminar and turbulent regions and are mainly noticeable in the laminar regime. First and foremost, there is a major difference of modelling that could explain this, since the heat flux  $\phi_w$  is directly computed from the enthalpy derivative close to the wall for the Neumann/Dirichlet coupling, see Eq. (19), while the convective heat exchange coefficient  $h_f$  is derived from  $C_f$  by the Reynolds analogy for the Robin/Dirichlet coupling. Moreover, the boundary condition  $h_f(x) (T_{aw}(x) - T_w(x))$  is adapting to  $T_w(x)$  variation at every iterations of the heat equation solver whereas for the Neumann/Dirichlet coupling the heat flux  $\phi_w$  is constant and only updated

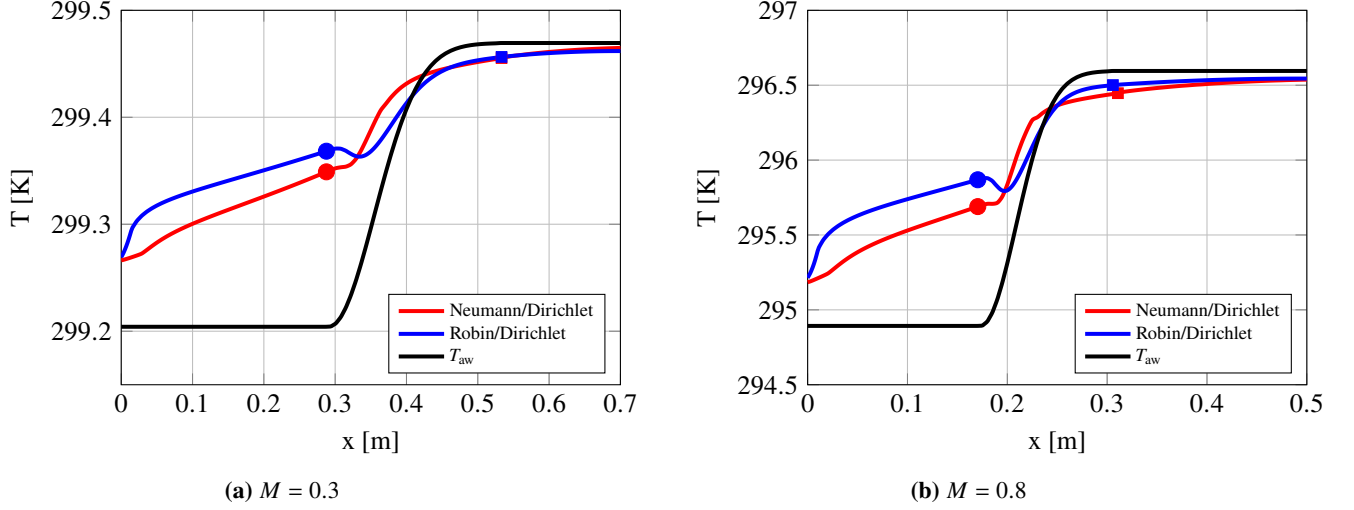


**Fig. 3** Comparison of temperature profile obtained with a Neumann/Dirichlet (solid red line) and a Robin/Dirichlet (solid blue line) coupling methods for two Mach number values. Circle symbols stand for the onset of transition while square symbols represent the end of the transitional region (*i.e.* the beginning of fully turbulent boundary-layer zone). The evolution of adiabatic wall temperature  $T_{aw}$  has been added for comparison and is depicted by the black full line.  $T_i = 300\text{K}$ ,  $P_i = 10^5\text{Pa}$ ,  $N_{TS} = 6$ ,  $k = 0.5\text{WK}^{-1}\text{m}^{-1}$ ,  $\varepsilon = 0.9$ ,  $T_{ray} = T_i$ .

after each call of the boundary-layer code. This is very likely to be responsible for the temperature difference in the laminar and transitional regimes. However in the turbulent regime, the heat flux  $h_f(x)$  ( $T_{aw}(x) - T_w(x)$ ) and  $\phi_w$  turn out to be very close, and so are the temperature profiles. Note that regardless of the modelling differences between the two couplings, the onset and end transition location are similarly predicted. Since the Robin/Dirichlet coupling is more efficient numerically, we decided to retain it for the rest of this study.

#### D. Unsteady computations

So far, only constant conditions have been considered, in order to calculate a steady state. However, it is also interesting to be able to calculate unsteady behaviors. Indeed, during experimental measurements, it is common to create a thermal disequilibrium by several means: switching on/off the cooling system of the wind tunnel, an IR lamp, an internal heating system by thermal resistance, etc...

There are two types of unsteady conditions: those specific to the flow ( $T_i$ ,  $P_i$ , Mach number) which are linked to the fluid solver, and those concerning the boundary conditions imposed on the structure (internal or external heat flux) linked to the solid solver. Of course, imposing unsteady conditions on the solid domain has repercussions on  $T_w$ , and thus influences the coupling with the fluid, and *vice versa*.

Numerically, we then move from a Backward Euler time scheme to a Crank-Nicholson scheme of order 2 in time ( $\theta = 0.5$ ), which thus requires a Fourier number  $Fo = \frac{k_m \Delta t}{\rho c_{pm} (\Delta L)^2}$  close to 0.5 to avoid numerical oscillations. The conductivity  $k_m$ , the thermal capacity  $c_{pm}$  and the density  $\rho_m$  are fixed by the material studied. The spatial discretisation size  $\Delta L$  is imposed by the mesh, and so the time step is set such as  $Fo = 0.5$ .

It therefore remains to set the number of time iterations  $n_t$  computed by the solid solver. It must be large enough, otherwise there is a risk of doing too many iterations, which would be numerically inefficient and costly. Nor can it be too large to have good temporal resolution. Moreover, the evolution of the conditions is only updated between two calls of the solid solver. At each call,  $n_t$  is adapted in order to meet these requirements.

The general idea of the unsteady coupling is similar to the steady Robin/Dirichlet coupling, except that the wall temperature is not initialized with  $T_i$  anymore, but with the temperature profile at equilibrium for the initial conditions. This requires to compute the steady state for these conditions using the steady Robin/Dirichlet coupling first.

#### IV. Guidelines for IR measurements

This section aims at giving guidelines to the experimenter who would like to perform IR measurements by studying the influence of different parameters of interest on the wall temperature in the academic framework of the flat plate using our Robin/Dirichlet coupling. Experimentally, there are several ways to define the transition position from a temperature profile measured by IR thermography. The two definitions mainly used place the transition position at 50% of the intermittency, or at the inflection point of the intermittency. In both cases, it is necessary to have a temperature gradient  $\Delta T$  between the laminar and turbulent zones as large as possible to limit the uncertainty on the determination of this transition position. It is with this aim that we study the efficiency of the main methods used in practice: addition of an insulating layer, use of an internal heating device or an IR lamp, thermal disequilibrium by switching on/off the cooling system of the wind tunnel.

The reference configuration is a flat plate consisting of a 20 mm aluminium layer covered with a 2 mm epoxy insulator of conductivity  $k_m = 0.5 \text{ WK}^{-1}\text{m}^{-1}$  (see Tab. 1) and emissivity  $\varepsilon = 0.9$  on which a transitional boundary layer develops. There is no inner or outer heating. The stagnation conditions are  $T_i = 300\text{K}$  and  $P_i = 10^5\text{Pa}$ , and the reference temperature of radiation is set to the stagnation temperature  $T_{\text{ray}} = T_i$ . The transition onset location is computed using the  $e^N$  method and the parabolas method, with  $N_{TS} = 6$  as transition threshold. Three Mach numbers will be considered from the subsonic regime  $M_0 = 0.3$  (corresponding to a unit Reynolds number  $Re = 6.30 \times 10^6 \text{ m}^{-1}$ ), to supersonic regime  $M_0 = 3$  ( $Re = 7.41 \times 10^6 \text{ m}^{-1}$ ), considering also transonic Mach number  $M_0 = 0.8$  ( $Re = 13.4 \times 10^6 \text{ m}^{-1}$ ). In the following, some parameters are made to vary in order to study their influence, but without explicit precision these sub-mentioned values are used as reference.

##### A. Influence of conductivity

The influence of the external layer material on the temperature gradient between laminar and turbulent zones  $\Delta T$  is studied. Figure 4 compares the listed materials in Tab. 1 for three Mach numbers. These materials have been identified by Gardner *et al.* [14] and considered to study the differential infrared thermography detection.

As it could be expected, the more insulating the material, the greater  $\Delta T$  since it reduces conduction which tends to

**Table 1 Thermal properties of the investigated materials constituting the external layer. From Gardner et al. [14], Bakelite has been added to have a material with a conductivity in the order of the unit,  $k_m = O(1)$ .**

Material	$k_m$ ( $\text{W m}^{-1} \text{K}^{-1}$ )	$c_{pm}$ ( $\text{J kg}^{-1} \text{K}^{-1}$ )	$\rho_m$ ( $\text{kg m}^{-3}$ )
Perfect Insulator	$10^{-5}$	1000	1000
Cork	0.05	1900	250
Polystyrene	0.1	1300	1100
Plexiglass	0.2	1500	1200
Epoxy	0.5	2300	1180
Bakelite	1.5	1500	1300
Lead	30	129	11340
Aluminium	300	900	2700

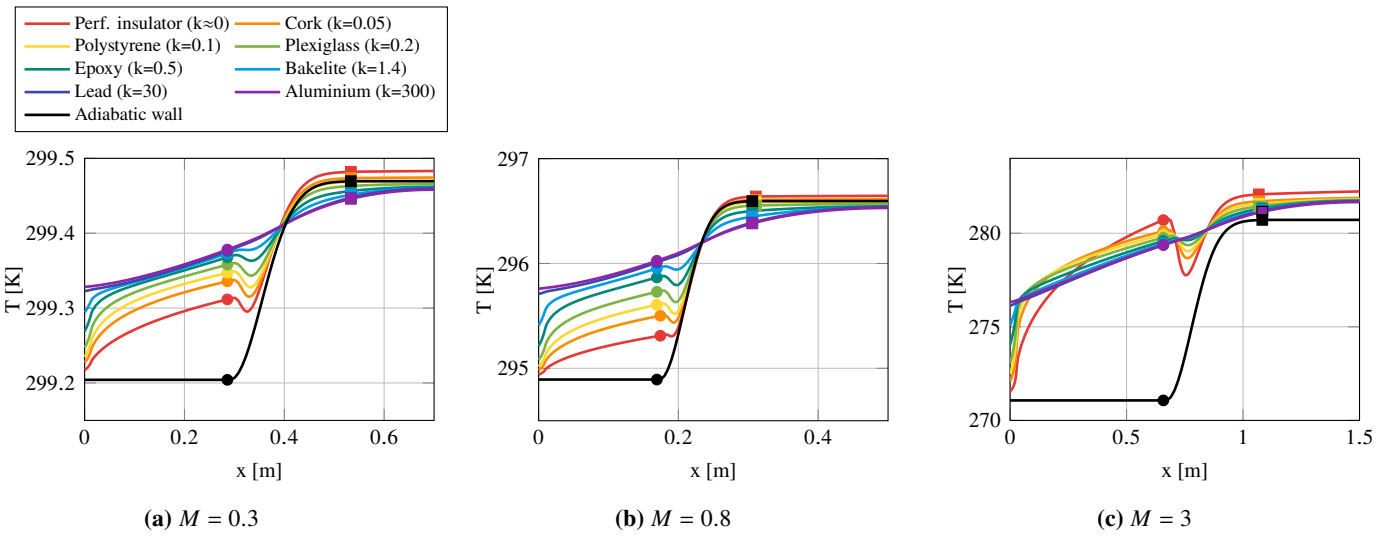


**Fig. 4 Comparison of the influence of the external layer thermal property on  $\Delta T$**

homogenize the wall temperature. For low Mach numbers, it is even more important to add a good insulator because the temperature gradient is lower than for supersonic regimes. For conductive materials (lead, aluminium), the temperature evolution is too smooth and it is practically impossible to detect the transition zone. We can also notice a slight drop in temperature at the beginning of the transition zone, referred as 'dip' or 'bucket'. This is sometimes observed experimentally especially in flight test conditions. Figure 20 in the appendix presents recent flight test results where this dip can be observed on a streamwise temperature profile. Further explanations can be found in the appendix.

## B. Influence of thickness

Figure 5 compares the influence of the epoxy layer thickness for several sub- trans- and super- sonic regimes with corresponding Mach numbers  $M = 0.3$ ,  $M = 0.8$  and  $M = 3$  respectively.

It is clear that the thickness of the insulation is as important as its conductivity on the evolution of surface temperature and allows to significantly increase the temperature gradient between the areas exposed to laminar or turbulent flows.

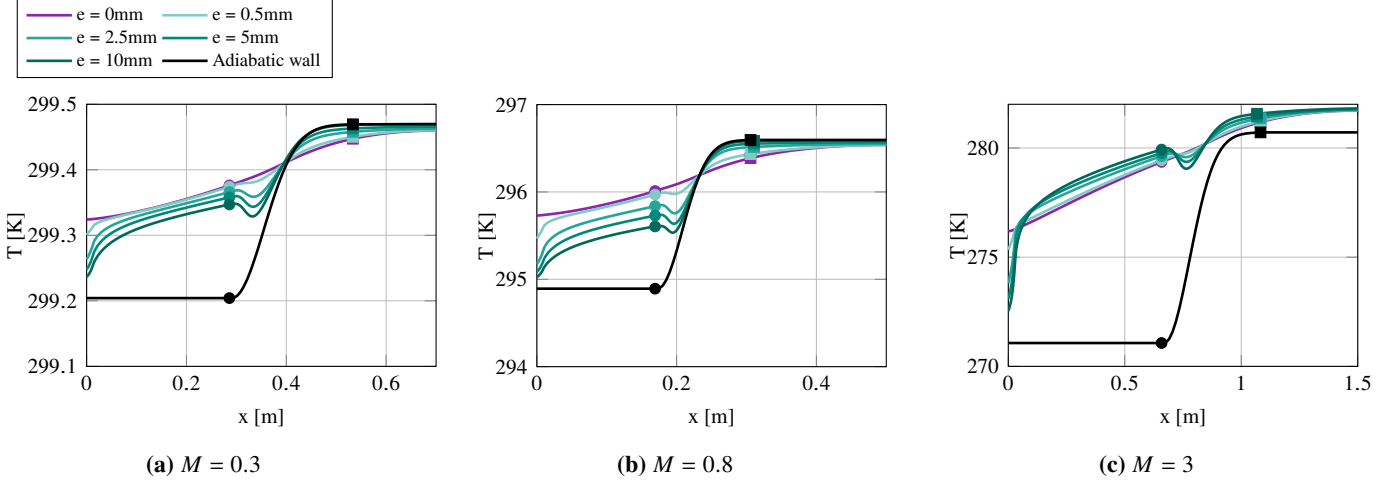


**Fig. 5 Comparison of the influence of the epoxy ( $k_m = 0.5\text{W m}^{-1}\text{K}^{-1}$ ) layer thickness on the wall surface temperature**

However, the thickness of this external material may be limited by structural and mechanical constraints.

As highlighted in figure 6, for a given  $k/e$ , the temperature profile remains constant. Under the stationary assumption without any source, equation (1) writes  $\Delta T = 0$ . Several quantities can be nondimensionalized as followed:  $T = \tilde{T}T^*$  with  $T^* = T_i$ ,  $y = \tilde{y}e$ ,  $\phi = \tilde{\phi}\phi^*$  and  $h = \tilde{h}h^*$ .

Equation (2) thus writes:

$$\frac{k}{e}T^* \left( \frac{\partial \tilde{T}}{\partial \tilde{y}} \right)_{\tilde{y}=0} = \tilde{\phi}\phi^* + \tilde{h}h^*T^* (T_{aw}^* - T_w^*) + \epsilon\sigma T^{*4} (T_{ray}^{*4} - T_w^{*4}) \quad (23)$$

Indeed, this equation depends on four different scales. If one of the parameters  $T^*$ ,  $\phi^*$  and  $h^*$  is modified, the temperature profile will be changed even for a given  $k/e$  ratio. On the contrary, if these three former parameters are fixed, the temperature profile will only depends on  $k/e$  as depicted in figure 6. Finally, figure 7 presents the evolution of wall temperature with  $k/e$  as a parameter for the three Mach numbers.

### C. Influence of a heating

To increase the temperature gradient at the transition, it is common to use heating devices. For example, IR lamps may be used to heat the outer wall (e.g. [12, 13, 34]), or wire heaters can be used to heat the inner wall (e.g. [13, 15, 16]). The influence of the internal/external flux supplied by these two methods is studied in figure 8.

First of all, one can notice that for an equal intensity, the wall temperature distributions obtained by an internal or an external flux are almost identical. This shows that the efficiency of these two methods is theoretically similar. This is consistent with our modeling of a flat plate without lateral heat loss and perfect contact resistance between the aluminium inner part and the insulating material, but this could be different for real cases. In practice, it is on the one hand more difficult to install an internal heating system, but on the other hand an external heating by IR lamp can cause

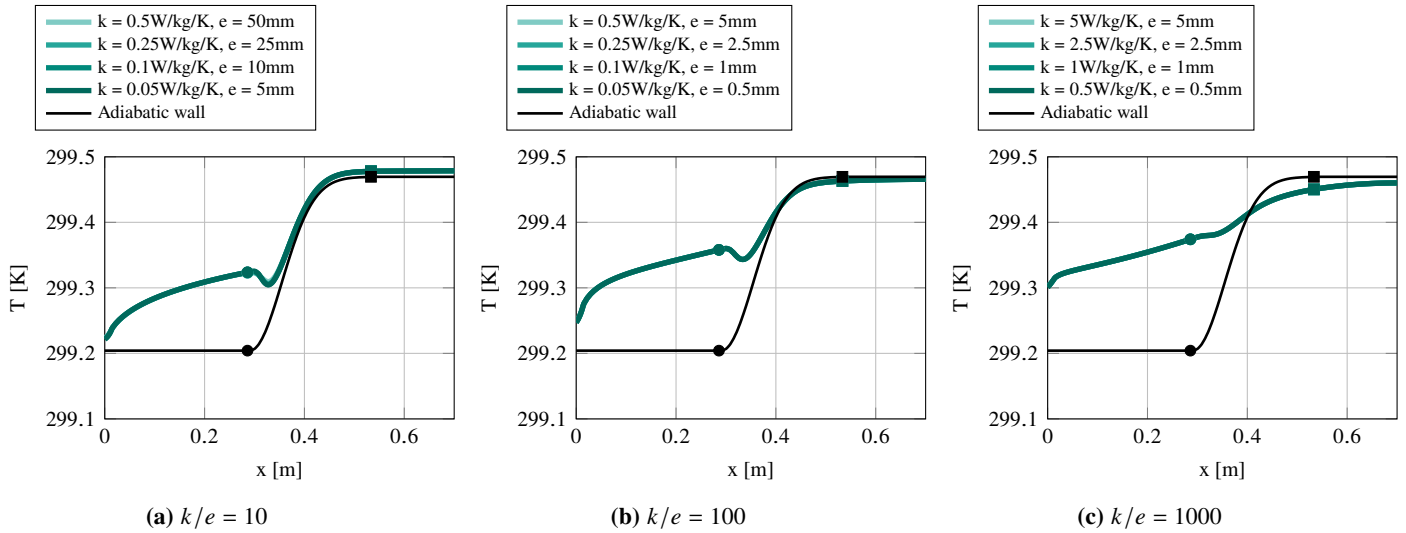


**Fig. 6** Comparison of the influence of the ratio  $k/e = 10, 100$  and  $1000 \text{ W m}^{-2} \text{ K}^{-1}$  on the wall surface temperature.

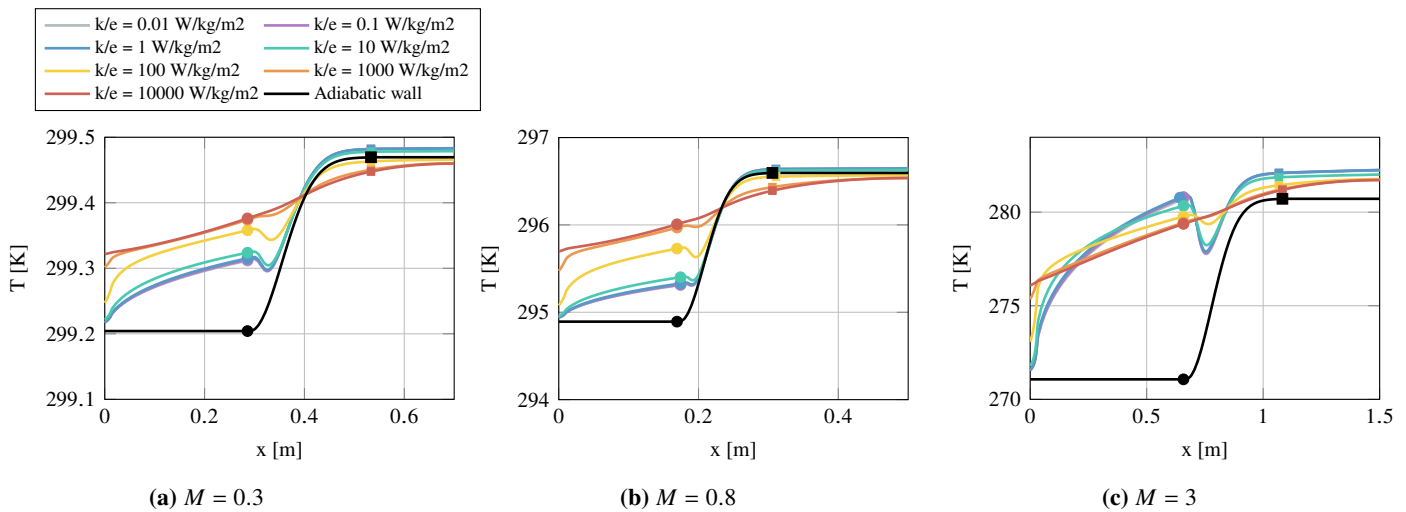


**Fig. 7** Comparison of the influence of the ratio  $k/e$  on the wall surface temperature for  $M = 0.3, 0.8$  and  $3$ .

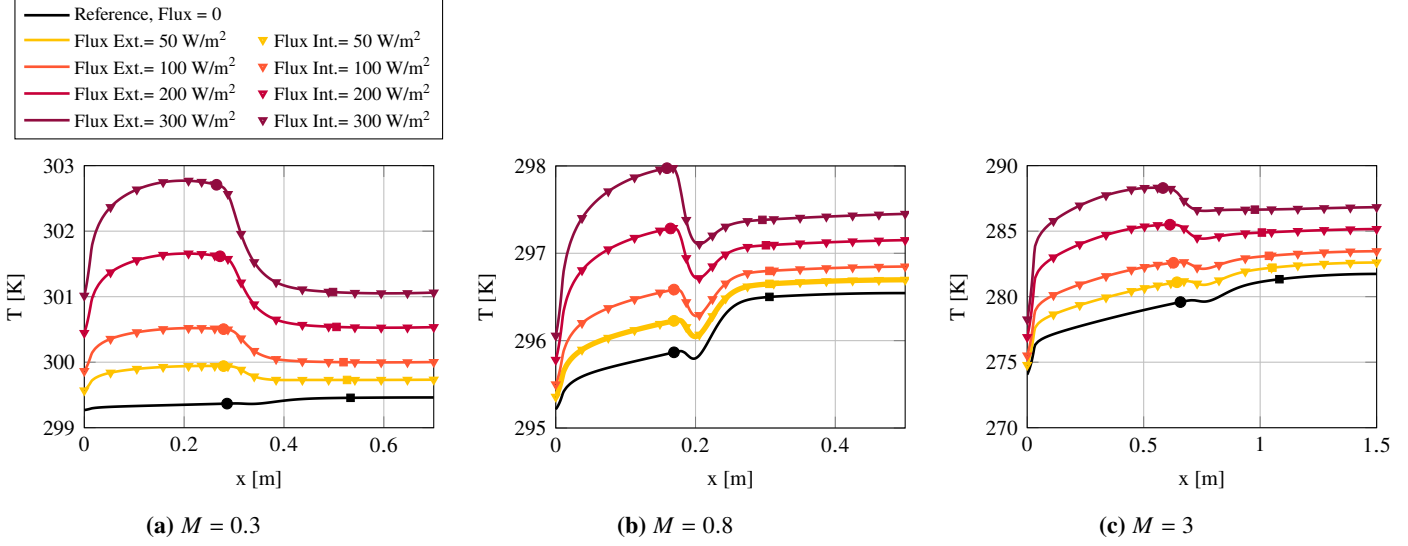


**Fig. 8 Comparison of the influence of an internal or external heating intensity on wall temperature distribution for  $M = 0.3, 0.8$  and  $3$ . Insulating material  $e = 2$  mm,  $k = 0.5 \text{ W m}^{-1} \text{ K}^{-1}$ .**

reflections and disturb the measurement and in case of close test section requires an ad-hoc window. An heating system can significantly increase the temperature gradient, as can be seen in for  $M = 0.3$  (8a) between the case  $\phi = 0$  and  $\phi = 300 \text{ W m}^{-2}$  where  $|\Delta T|$  increases from  $0.1$  K to  $2$  K. In addition, it seems that the laminar zone is more sensitive to heat flux. If initially the laminar zone is colder than the turbulent zone, this can allow the gradient to be reversed and have a laminar zone that becomes warmer than the turbulent zone. If the laminar zone is already warmer, the heating system can further increase the gradient.

The unsteady effects of an internal/external heating are also investigated using the Robin/Dirichlet unsteady coupling. The initial conditions are the reference conditions, without any heating and a Mach number  $M = 0.8$ . At  $t = 1$  s, a thermal disequilibrium is triggered by the sudden variation of the heating intensity:

- Case 1: external heating  $\phi_{ext} = 300 \text{ W m}^{-2}$ , corresponding to switching on an IR lamp (see figure 9a),
- Case 2: internal heating  $\phi_{int} = 300 \text{ W m}^{-2}$ , corresponding to switching on an internal heating system (see figure 9b).

The purpose is to determine whether during the transient state due to a change in the intensity of the supplied heat flux, the temperature gradient increases significantly over a certain period of time. For the considered cases, the temperature profile undergoes a gradient inversion between the initial and final state since the laminar zone is more sensitive than the turbulent zone to the heat flux. Thus, during most of the transient state, the temperature of the laminar zone approaches that of the turbulent zone, and the temperature gradient decreases. The temperature gradient is maximal at the final state, so that for this example, make measurements during the transient state is not interesting since the laminar zone is initially colder than the turbulent zone. Note that for an internal heating, the onset of the evolution of the wall temperature is delayed of a few seconds (see green curves of figures 9a and 9b corresponding to

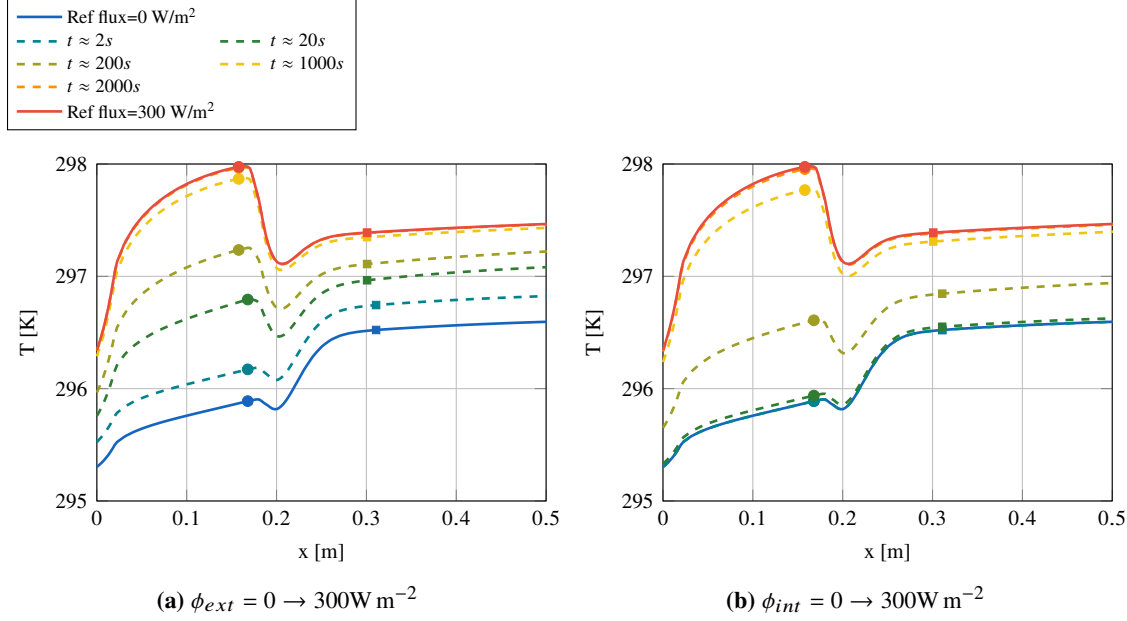


**Fig. 9** Investigation of the unsteady effects of an internal/external heating by applying a thermal disequilibrium at  $t = 1$ s from an initial state without any heating at  $M = 0.8$ . Comparison to the initial and final states computed using the Robin/Dirichlet steady coupling

$t \approx 2$  s and  $t \approx 20$  s) due to the heat diffusion time between the inner and outer surface, which is for a 2 mm layer of epoxy  $\tau \approx \frac{\rho_m c_{pm} e^2}{k_m} = 21.7$  s. This is also illustrated in figure 10 where the time evolution of the temperature difference between the laminar and turbulent region is represented.

If the wall is pre-heated so that the laminar zone is warmer, and then the heat flux is increased, the temperature difference between laminar and transition zone is lower than the value reached when thermal equilibrium is effective. Figure 11 shows a case where an initial internal heating of  $\phi_{int} = 300$ W m<sup>-2</sup> contributes to have a laminar zone warmer. The heating is then increased to  $\phi_{int} = 500$ W m<sup>-2</sup>, but the greater temperature difference is still obtained in the final state.

#### D. Influence of a thermal disequilibrium

During wind tunnel testing, it is common to turn on/off the cooling system in order to change the stagnation temperature  $T_i$  of the fluid and thus create a greater thermal imbalance with the model. The case of a thermal disequilibrium at  $M = 0.8$  where  $T_i$  falls from 300K to 295K, or rises from 300 K to 305 K is investigated in figure 12.

The modification of the stagnation temperature modifies the absolute level of the wall temperature distribution, which remains almost identical from a relative point of view: the initial  $\Delta T$  is more or less identical to the final  $\Delta T$ . This is consistent with the fact that for a given Mach number,  $T_{aw}$  is linearly linked to  $T_i$ , so the difference of  $T_{aw}$  in the laminar and turbulent regimes is unchanged. However, the turbulent regime is more sensitive than the laminar zone to thermal disequilibrium and the temperature in this zone varies more quickly, which allows to obtain a higher  $\Delta T$  during

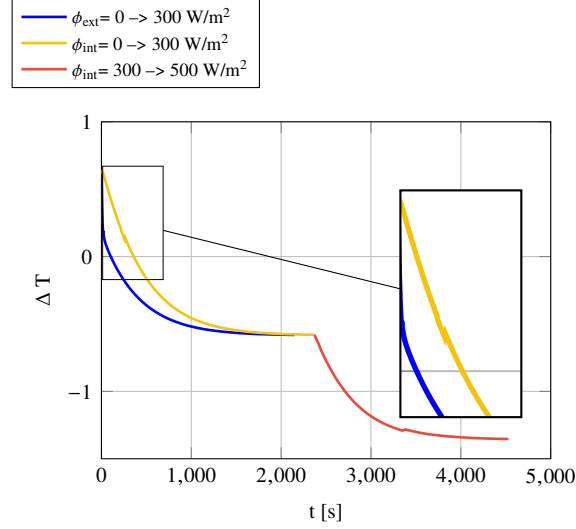


**Fig. 10 Evolution of wall temperature during transient state for 3 distinct flux condition based on a thermal disequilibrium at  $t = 1$  s. Blue curve  $\phi_{ext} = 0 \rightarrow 300 \text{ W m}^{-2}$  (corresponding to figure 9a), orange curve  $\phi_{int} = 0 \rightarrow 300 \text{ W m}^{-2}$  (corresponding to figure 9b), red curve  $\phi_{int} = 300 \rightarrow 500 \text{ W m}^{-2}$  (corresponding to figure 11). Since the initial stage of red curve corresponds to the final one of the orange curve, the time reference has been shifting accordingly.**

the transient regime.

In figure 12a, the temperature undergoes a gradient inversion during the transient state and the maximum gradient during the transient state is about  $\Delta T \approx 1.5$  K, unlike in figure 12b in which there is no gradient inversion and the maximum gradient is  $\Delta T \approx 2.5$  K. The time evolution of wall temperature for these both cases is depicted in figure 13. During the transition phase, the maximum wall temperature difference between the laminar and turbulent region is reached very quickly around  $t_{\Delta T_{\max}} \approx 17$  s when the stagnation temperature is increased and  $t_{\Delta T_{\max}} \approx 16$  s when  $T_i$  decreases. There is therefore a real interest in using this kind of method, already well known by experimenters, and especially when the temperature gradient between the laminar and turbulent regimes does not reverse. Nonetheless, in the current simulations, the total temperature value is abruptly changed which may not be representative of the evolution of  $T_i$  during wind tunnel testing when the cooling system is switched on/off and where a more progressive evolution of the stagnation temperature is expected. Such real configurations will be investigated in more details in section V.

This can be explained by noting that  $T_{aw}$  is linearly dependent on  $T_i$ , and that for a small variation of  $T_i$  the flow properties are expected to be little changed, and therefore  $h_f$  can be assumed to be almost unchanged. But since  $h_f^{turb} > h_f^{am}$ , the convective term  $h_f(T_{aw} - T_w)$  is more intense in the turbulent than in the laminar zone and the temperature varies more abruptly during the transient state. With these same arguments, we can explain why in the previous case (IV.C Influence of a heating), the laminar zone was more sensitive than the turbulent zone to the contribution of a global external/internal heat flux: without modification of  $T_i$ , and thus of  $T_{aw}$  and  $h_f$ , the convective term acts as a less intense recovery source in the laminar zone, and this one evolves therefore faster during the transient

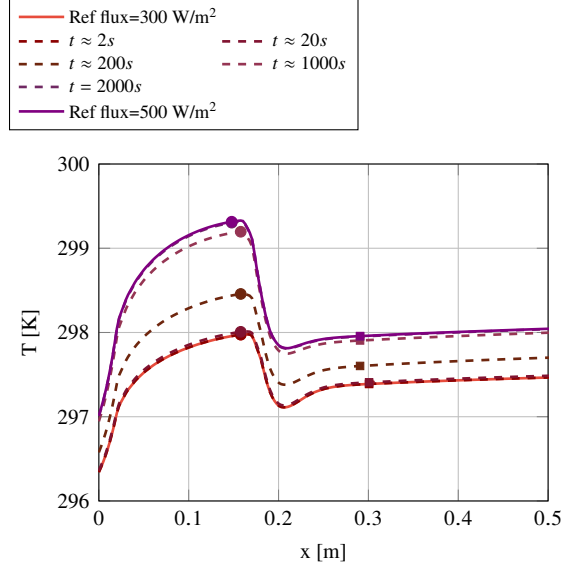


**Fig. 11 Investigation of the unsteady effects of an internal heating by applying a thermal disequilibrium at  $t = 1$  s from an initial state with  $\phi_{int} = 300 \text{ W m}^{-2}$  to  $\phi_{int} = 500 \text{ W m}^{-2}$  at  $M = 0.8$  (corresponding to the final stage of figure 9b. Comparison to the initial and final states computed using the Robin/Dirichlet steady coupling**

state.

## V. Application on real cases

In this section, the Robin/Dirichlet with Reynolds analogy coupling code is applied to a real model tested at the S2MA (Soufflerie 2 Modane Avrieux) wind tunnel.

### A. Application to wind-tunnel tests: transonic airfoil

In order to apply the code on real configurations, we want to compare the numerical predictions with experimental measurements. The model considered is a laminar symmetrical airfoil made of aluminium, to which a 1mm layer of highly insulating ( $k \approx 0.05 \text{ W m}^{-1} \text{ K}^{-1}$ ) and anti-reflective ( $\varepsilon \approx 0.9$ ) epoxy resin have been added. The tests were conducted in the transonic regim at the S2MA, a pressurized closed- circuit wind tunnel of ONERA at the Modane-Avrieux centre. The profile chord is  $c = 0.396 \text{ m}$ . Figure 14 shows the airfoil which has been designed to be a laminar symmetric profile. The pressure coefficients, denoted  $K_p$  are plotted in figure 14, for  $P_i = 1 \text{ bar}$ ,  $T_i = 308.6 \text{ K}$  and  $M = 0.8$  and zero angle of attack.

The model wall temperature is measured using IR thermography on the suction side. The IR camera has been preliminary calibrated thanks to a black body. An example of raw IR image is represented in figure 15. On this figure, the transition line has been determined at the location of the inflexion point of the chordwise temperature profile and is represented by the solid black line.

A first challenge is to reproduce these test conditions numerically, since at the time of the measurement the model

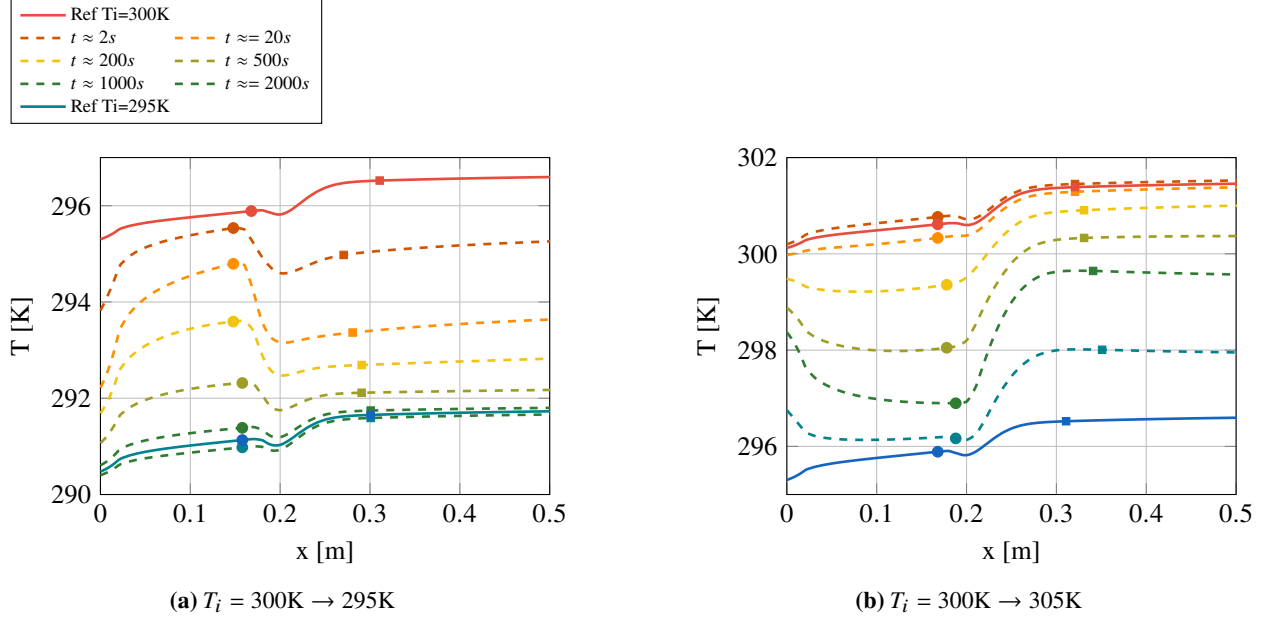


**Fig. 12** Investigation of the unsteady effects of a thermal disequilibrium at  $t = 1\text{s}$  from an initial state at  $M = 0.8$  and  $T_i = 300\text{K}$ . Comparison to the initial and final states computed using the Robin/Dirichlet steady coupling.

was not in a thermal stationary state. In fact, the experimenters are constantly changing the total temperature of the flow by switching on/off the cooling system so as to increase the thermal imbalance between the flow and the model, and improve IR image contrast. In order to numerically reproduce as faithfully as possible the test conditions, the calculation is initialized with a constant temperature value in the whole volume of the model corresponding to the mean value of the wall temperature measured by IR thermography during the previous operating point. For each operating point, the total temperature is measured as well as the corresponding time. Therefore, starting from this initial state, an unsteady Robin/Dirichlet coupling is performed to compute the wall temperature, with  $T_i$  evolving linearly from 306K to 308.6K in 4 minutes. An  $e^n$  method with parabolax method is used to compute the transition onset. Since the wing has a zero-sweep angle, the transition is only triggered by TS waves and occurs when the N-factor exceeds a given limit  $N_{TS} = 6.3$ . This value is imposed by the characteristics of the S2MA wind-tunnel. The turbulence rate measurements integrated on a large frequency bandwidth (from 3Hz up to 20kHz) provides a typical value of  $Tu = 0.22\%$  for Mach number  $M = 0.8$  which corresponds to a critical N-Factor  $N_{Mack} = 6.3$  (based on Equation 12) and  $Tu = 0.21\%$  for  $M = 0.7$  corresponding to  $N_{Mack} = 6.4$ . The critical N-factors obtained by the  $e^n$  method with transition measurements from IR images and the one given by the Mack law using the measured turbulence level are consistent.

The chordwise evolution of the wall temperature is extracted along the  $y = 25\text{mm}$  line from the IR image (dashed line in figure 15) and compared to the numerical one in figure 16. A global deviation of 2.4K is found between the measurements (bright blue circles) and the numerical results (red curve). However if one adds this difference from the measured temperature distribution (blue curve), one can notice that the relative effects are consistent regarding

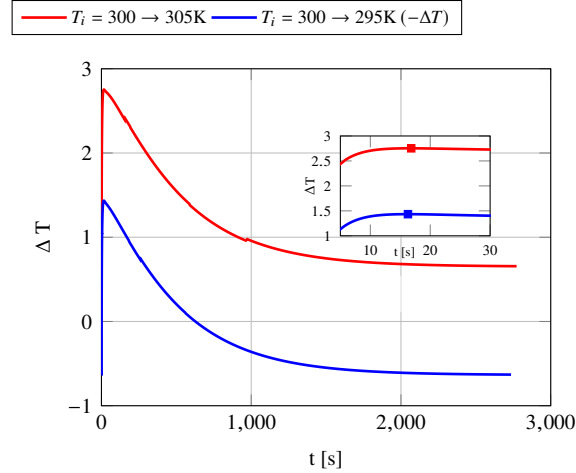


**Fig. 13** Evolution of wall temperature during transient state when total temperature is abruptly modified at  $t = 1$  s. Blue curve  $T_i = 300 \rightarrow 295\text{K}$ , red curve  $T_i = 300 \rightarrow 305\text{K}$ .

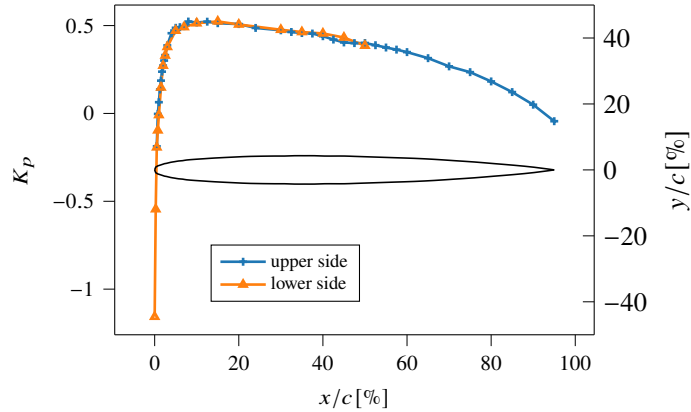


**Fig. 14** Airfoil profile and measured pressure coefficient suction side (blue line) and pressure side (orange line) for  $P_i = 1\text{bar}$ ,  $T_i = 308.6\text{K}$  and  $M = 0.8$  test case ( $Re_c \approx 5 \times 10^6$ )

the temperature difference between the laminar and turbulent regime. Concerning the transition, the onset location and intermittency are highly accurate, which support our choice of Dhawan and Narasimha intermittency function. In practice, the most important is to predict the transition area and temperature difference between the laminar and turbulent regimes, first to guarantee that transition will occur, and above all to ensure that the temperature variation is sufficient to have high quality IR measurements.

### B. Wind-tunnel operation strategies to obtain valuable IR images for transition onset measurements

While operating wind-tunnel test for laminarity studies, several "know-how" hints are required to have a significant thermal gradient due to transition onset in order to identify easily and accurately the transition onset position. Several wind-tunnel operating strategies are simulated thanks to the aerothermal approach described before. In practice, the wind-tunnel test engineer can both increase or decrease the Mach number or/and act on the wind-tunnel cooling system.

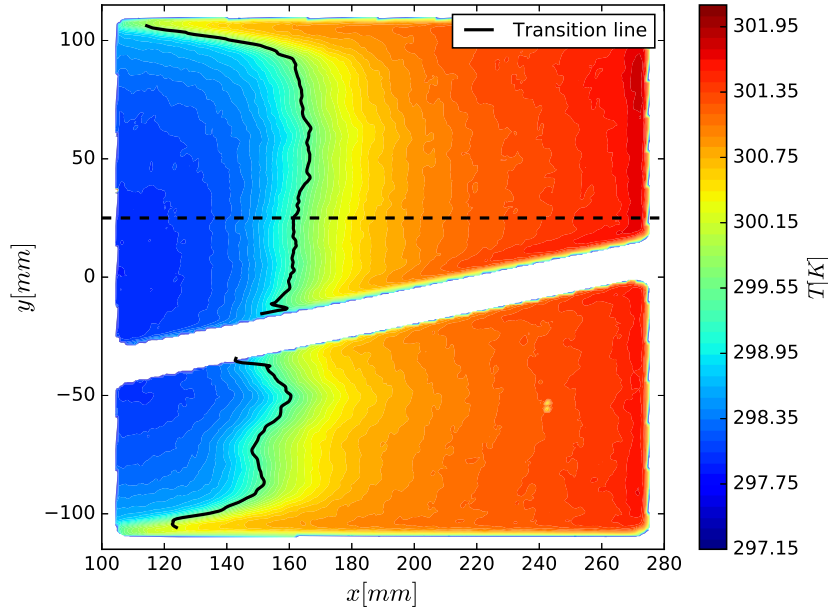


**Fig. 15** IR thermography measurements of the model at S2MA and detection of the transition line -  $P_i = 1\text{bar}$ ,  $T_i = 308.6\text{K}$  and  $M = 0.8$  ( $Re_c \approx 5 \times 10^6$ ).

While the test engineer must fulfill the customer/researcher test matrix, he must ensure high quality IR images with a sufficient contrast to enable interpretations. The idea is thus to find the right way of operating the wind-tunnel in order to achieve some condition variation in adequation with the test matrix. The present study enables to simulate these operating strategies and thus gives insights in order to optimize the test. Figure 17a presents the surface temperature profile calculation compared to the experimental results when the conditions are suddenly modified. The initial state is extracted from the previous measurement point conditions (uniform temperature at  $t = 0$ ). The Mach number change is assumed to be instantaneous while the total temperature modification is progressively imposed through linear variation. The final state ( $t = 180\text{s}$ ) is thus compared to the experimental results and the agreement is fairly good after the measurements have been shifting with a constant offset. Figure 17b presents the same kind of results when a decrease of the Mach number, the temperature and the total pressure is applied. The initial gradient ( $t = 0$ ) is similar to the one observed in figure 17a with a laminar zone colder than the turbulente one. After a long time ( $t = 780\text{s}$ ), the final temperature profile has an reverse gradient (laminar zone warmer than the turbulente one) which is in very good agreement with the experimental results. The aerothermal approach catches very well this typical behaviour that one can meet during such a test. This strategy remains interesting for the objectives of having the best IR measurement but one can notice that it takes a lot of time to reach this reverse gradient. Finally, figure 17c presents an increase from low subsonic Mach number where the gradient is usually insufficient to identify the transition position to higher Mach number while the total temperature increases in the same time. This operating strategy is very efficient in order to

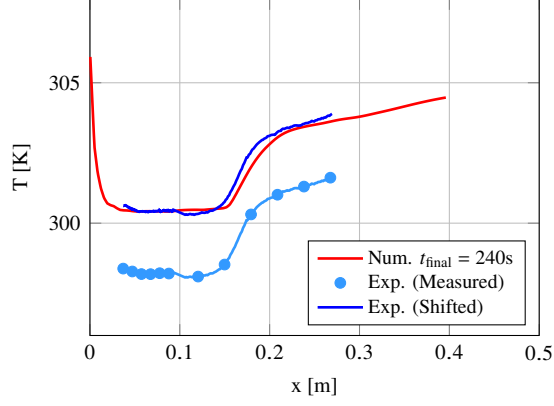


**Fig. 16 Comparison of the experimental and numerical wall temperature chordwise extracted on the  $y = 25\text{mm}$  line for the application case.  $P_i = 1\text{bar}$ ,  $T_i = 308.6\text{K}$  and  $M = 0.8$  ( $Re_c \approx 5 \times 10^6$ ).**

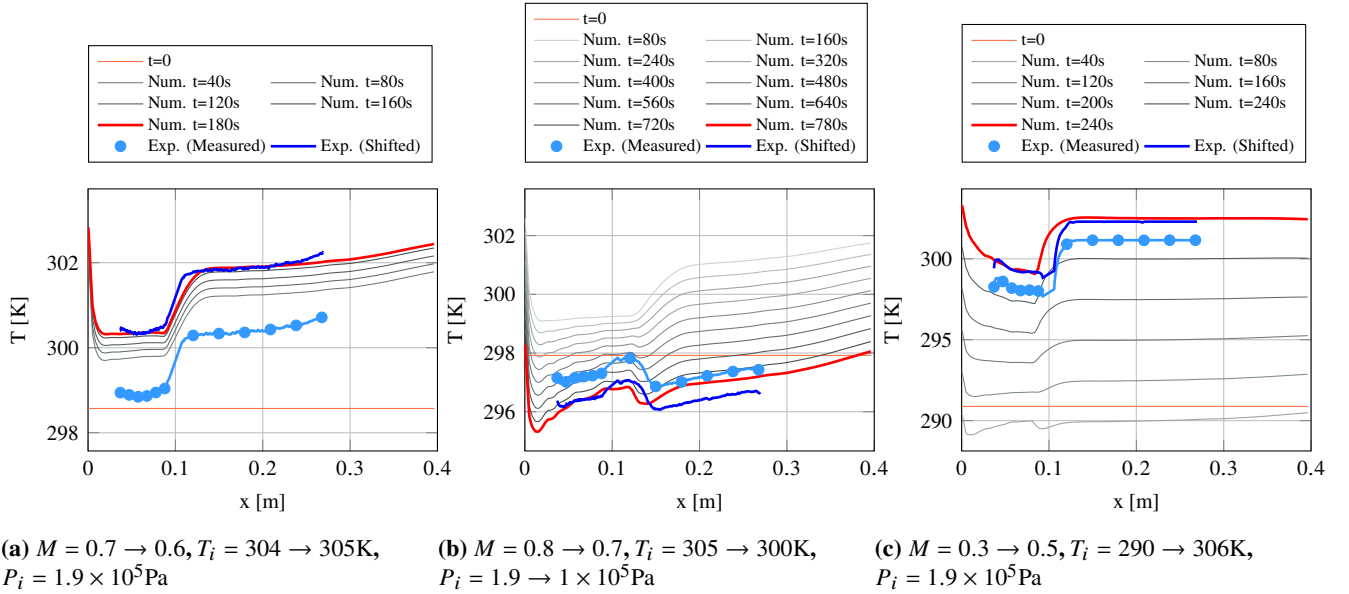


**Fig. 17 Unsteady surface temperature profile evolution for different flow conditions variations**

improve the temperature gradient. The present aerothermal calculations reproduce well the impact of the flow condition variations and thus can be considered as a valuable tool for the preparation phase of wind-tunnel test.

## VI. Conclusion

A numerical coupling between two codes solving the boundary-layer equations for the fluid and heat equation for the solid is presented. Several coupling approaches have been investigated and discussed in the article. The most efficient coupling strategy has been retained: it is based on a Robin boundary condition involving the Reynolds analogy relation. Unsteady computations are possible considering changes in fluid conditions (Mach number, total temperature and total pressure) as well as in the solid (heat flux) taking into account all the physics involved in such a change. The use of

the aerothermal coupling in the academic framework of the flat plate allowed to determine the influence of several parameters on the temperature gradient between the laminar and turbulent zone, and thus to give basic guidelines to the experimenter. Numerical analysis has demonstrated a good predictive behaviour compared to wind-tunnel transonic experimental results. It represents a useful tool to design model (properties and thickness of insulating material, internal heating device, ...) as well as to define aerodynamic conditions (variation of total temperature, external flux, ...) to be set-up for measurements of laminar-turbulent transition in wind-tunnel or flight tests using an infra-red camera. A major improvement of the method applied in this article would be to get rid of the Reynolds analogy assumption which links the friction coefficient to the heat transfer coefficient. This would allow to take full advantage of the coupling between the two codes and would be closer to physics. This could be done at least by two different formulations. First, considering the Robin/Dirichlet coupling, the heat transfer coefficient  $h_f$ , was not directly computed through its definition  $h_f = q/(T_w - T_{aw})$  with  $q = k_f(\partial T/\partial y)_{y=0}$  but deduced from the heat transfer coefficient  $C_h$  using the Reynolds analogy. This has been done due to convergence issues when the wall temperature get closer to the adiabatic one. An alternative should be to use a two temperatures strategy [17] consisting in performing an additional fluid computation with an other *arbitrary* surface temperature  $T_{w,2}$  and compute the heat transfer coefficient using the relation  $h = (q - q_2)/(T_w - T_{w,2})$ . Another possibility would be to come back to the Neumann/Dirichlet formulation and use the *numerical Biot number* approach developed by Moretti et al. [35] to improve the efficiency and the stability of the coupling. This tool can easily be extended to 3D test cases, but stays limited to flow conditions without boundary-layer separation (due to limitations of the boundary-layer solver). Several transition scenarii can also be considered (bypass or crossflow transition) as long as the boundary-layer solver models them. Additionally, taking into account more elaborate turbulence models would allow improvement in turbulent flow regime.

## Appendix

To explain the existence of the bucket at the beginning of the transition region, let's consider the simplified case of a flat plate made of a perfect isolating material ( $k_m \rightarrow 0$ ) without any external flux ( $\Phi = 0$ ). For such a case, the wall temperature results from the competitive effect of convection which tends to attract the wall temperature  $T_w$  towards the adiabatic wall value  $T_{aw}$  and the radiation phenomenon which forces  $T_w$  to  $T_{ray}$ . The wall temperature is determined by the boundary equation (2) which simplifies as:

$$h_f(x) (T_{aw}(x) - T_w(x)) + \epsilon\sigma (T_{ray}^4 - T_w^4(x)) = 0 \quad (24)$$

All along the laminar region (from  $x = 0$  to 0.5), the adiabatic wall temperature  $T_{aw}$  remains constant as depicted in figure 18 (blue curve) while the convective heat coefficient  $h_f$  decreases up to its minimum value at the transition onset starting point at  $x = 0.5$  (red curve). In the same time, the radiative source term ( $\epsilon\sigma T_{ray}^4$ ) keeps unchanged so that, as

$(h_f T_{aw})$  decreases, it becomes more and more important in the equilibrium balance. Therefore, as in the considered case  $T_{ray} > T_{aw}$ , this leads to an increase of the wall temperature in the laminar region. Such effect being all the more significant than the heat transfer by radiation is important. This is well illustrated in figure 19 where the intensity of radiation transfer is varied by modifying the value of the emissivity from  $\epsilon = 0.9$  (important effect) to 0.1 (small effect). When the emissivity is weak (green curve,  $\epsilon = 0.1$ ), the wall temperature is very close to the adiabatic wall temperature (bright blue curve).

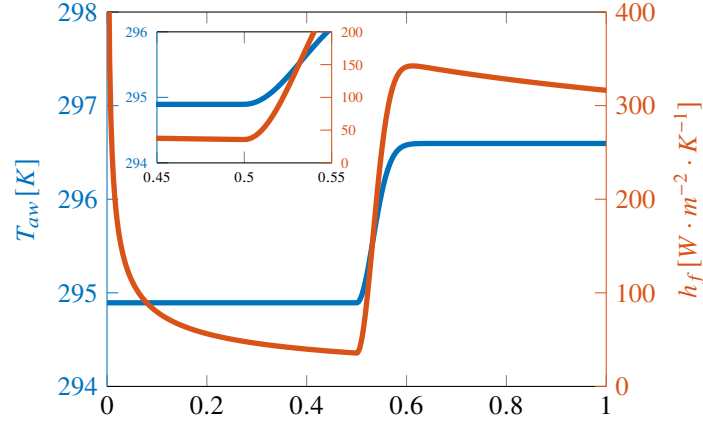


**Fig. 18** Streamwise evolution of the adiabatic wall temperature and convective heat transfer for a flat plate made of a perfect insulating material ( $k_m \rightarrow 0$ ) submitted to an external flow characterized by  $M = 0.8$ ,  $P_i = 10^5$  Pa and  $T_i = 300$  K. The radiation temperature is set-up to  $T_{ray} = T_i = 300$  K, the emissivity to  $\epsilon = 0.9$  and the transition is imposed at  $x = 0.5$ . A magnified view of the transition region has been added.

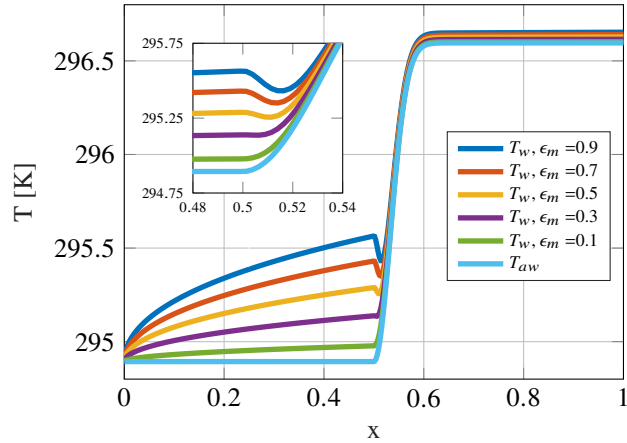


**Fig. 19** Streamwise evolution of the wall temperature as a function of the magnitude of the radiative heat transfer which is varied through  $\epsilon$  values from 0.9 to 0.1. Same conditions as in figure 18. A magnified view of the transition region has been added.

At the transition onset, the convection coefficient  $h_f$  abruptly raises (see the red curve of figure 18 at  $x = 0.5$ ) imposing an intense recall for the wall temperature towards the adiabatic one which is in our case lower than  $T_w$ . This leads to a decrease of  $T_w$  so that, as the difference  $(T_{ray} - T_w)$  increases, the radiation term is enhanced and partly

counterbalances the wall temperature cooling due to the sudden change of the convective heat coefficient. In the same time,  $T_{aw}$  raises, gets closer to  $T_w$  and finally higher than its value in the laminar zone leading eventually to an increase of the wall temperature.

In conclusion, the bucket is a transient state which results from an initial wall temperature increase due to radiation in the laminar zone leading to a non negligible difference between wall and adiabatic wall temperature. At the transition starting point, a sudden increase of the convective heat coefficient imposes a recall of the wall temperature towards the adiabatic one before raising again. This bucket may be observed experimentally as represented in figure 20 corresponding to flight test measurement. For this case, the bucket (see the magnified view between  $x = 0.25$  and  $x = 0.45$  in figure 20, is due to a competitive effect between convection and solar heat flux.

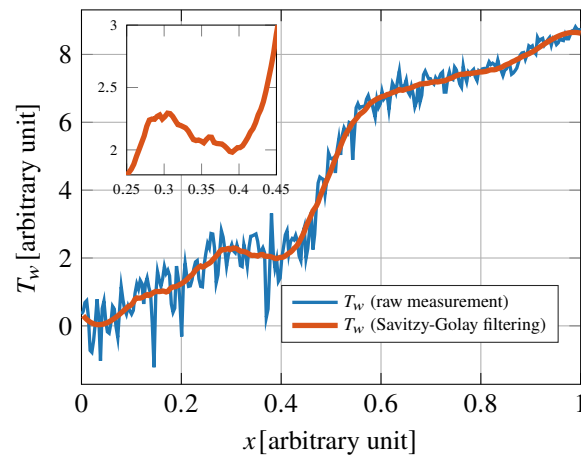


**Fig. 20 Streamwise evolution of the wall temperature during transonic flight test experiment (raw and filtered data). A magnified view of the transition region has been added.**

## Acknowledgments

This work has been partly funded within the frame of the Joint Technology Initiative JTI Clean Sky 2, AIRFRAME Integrated Technology Demonstrator platform "AIRFRAME ITD" (contract CSJU-CS2-GAM-AIR-2020-945521) being part of the Horizon 2020 research and Innovation framework programme of the European Commission."

## References

- [1] Arnal, D., and Archambaud, J., "Laminar-Turbulent Transition Control: NLF, LFC, HLFC," *Advances in Laminar-Turbulent Transition Modeling, VKI Lecture Series*, Brussels, 2008.
- [2] Schubauer, G., and Skramstad, H., "Laminar boundary-layer oscillations and stability of laminar flow," *Journal of the Aeronautical Sciences*, Vol. 14, No. 2, 1947, pp. 69–78. <https://doi.org/10.2514/8.1267>.
- [3] Costantini, M., Henne, U., Risius, S., and Klein, C., "A robust method for reliable transition detection in temperature-sensitive

- paint data,” *Aerospace Science and Technology*, Vol. 113, 2021, p. 106702. <https://doi.org/https://doi.org/10.1016/j.ast.2021.106702>.
- [4] Le Sant, Y., Marchand, M., Millan, P., and Fontaine, J., “An overview of infrared thermography techniques used in large wind tunnels,” *Aerospace Science and Technology*, Vol. 6, 2002. [https://doi.org/10.1016/S1270-9638\(02\)01172-0](https://doi.org/10.1016/S1270-9638(02)01172-0).
- [5] Wolf, C. C., Gardner, A. D., and Raffel, M., “Infrared thermography for boundary layer transition measurements,” *Measurement Science and Technology*, Vol. 31, No. 11, 2020, p. 112002. <https://doi.org/10.1088/1361-6501/aba070>.
- [6] Thomann, H., and Frisk, B., “Measurement of heat transfer with an infrared camera,” *International Journal of Heat and Mass Transfer*, Vol. 11, No. 5, 1968, pp. 819–826. [https://doi.org/10.1016/0017-9310\(68\)90126-9](https://doi.org/10.1016/0017-9310(68)90126-9).
- [7] Bouchardy, A., and Durand, G., “Processing of infrared thermal images for aerodynamic research,” *Applications of Digital Image Processing V*, Vol. 397, International Society for Optics and Photonics, 1983, pp. 304–309. <https://doi.org/10.1117/12.935316>.
- [8] Quast, A., “Detection of Transition by Infrared Image Technique, ICIASF’87 Record,” *IEEE Publication*, 1987.
- [9] Banks, D., van Dam, C., Shiu, H., and Miller, G., “Visualization of in-flight flow phenomena using infrared thermography,” Tech. rep., National Aeronautics and Space Administration, Dryden Flight Research Center, 2000.
- [10] Crawford, B., Duncan Jr, G., West, D., and Saric, W., “Laminar-turbulent boundary layer transition imaging using IR thermography,” *Optics and Photonics Journal*, Vol. 3, No. 03, 2013, p. 233. <https://doi.org/10.4236/opj.2013.33038>.
- [11] Zuccher, S., and Saric, W., “Infrared thermography investigations in transitional supersonic boundary layers,” *Experiments in Fluids*, Vol. 44, No. 1, 2008, pp. 145–157. <https://doi.org/10.1007/s00348-007-0384-1>.
- [12] Raffel, M., and Merz, C., “Differential infrared thermography for unsteady boundary-layer transition measurements,” *AIAA journal*, Vol. 52, No. 9, 2014, pp. 2090–2093. <https://doi.org/10.2514/1.J053235>.
- [13] Simon, B., Filius, A., Tropea, C., and Grundmann, S., “IR thermography for dynamic detection of laminar-turbulent transition,” *Experiments in Fluids*, Vol. 57, No. 5, 2016, p. 93. <https://doi.org/10.1007/s00348-016-2178-9>.
- [14] Gardner, A., Eder, C., Wolf, C., and Raffel, M., “Analysis of differential infrared thermography for boundary layer transition detection,” *Experiments in Fluids*, Vol. 58, No. 9, 2017, pp. 1–14. <https://doi.org/10.1007/s00348-017-2405-z>.
- [15] Joseph, L., Borgoltz, A., and Devenport, W., “Infrared thermography for detection of laminar–turbulent transition in low-speed wind tunnel testing,” *Experiments in Fluids*, Vol. 57, No. 5, 2016, p. 77. <https://doi.org/10.1007/s00348-016-2162-4>.
- [16] Crawford, B., Duncan, G., West, D., and Saric, W., “Robust, automated processing of IR thermography for quantitative boundary-layer transition measurements,” *Experiments in Fluids*, Vol. 56, No. 7, 2015, pp. 1–11. <https://doi.org/10.1007/s00348-015-2011-x>.
- [17] Verdicchio, J., Chew, J., and Hills, N., “Coupled fluid/solid heat transfer computation for turbine discs,” *Volume 3: Heat Transfer; Electric Power; Industrial and Cogeneration*, Turbo Expo: Power for Land, Sea, and Air, 2001. <https://doi.org/10.1115/2001-GT-0205>.

- [18] Heidmann, J., Kassab, A., Divo, E., Rodriguez, F., and Steinhilber, E., “Conjugate heat transfer effects on a realistic film-cooled turbine vane,” *Volume 5: Turbo Expo 2003, Parts A and B*, Turbo Expo: Power for Land, Sea, and Air, 2003, pp. 361–371. <https://doi.org/10.1115/GT2003-38553>.
- [19] Verstraete, T., Alsalihi, Z., and Van der Braembussche, R., “A Conjugate heat transfer method applied to turbomachinery,” *Proceedings of the European Conference on Computational Fluid Dynamics*, edited by P. Wesseling, E. Oñate, and J. Périaux, ECCOMAS CFD 2006, 2006.
- [20] Radenac, E., “Développement et validation d’une méthode numérique pour le couplage fluide/structure en aérothermique instationnaire,” Ph.D. thesis, Toulouse, ENSAE, 2006.
- [21] Reulet, P., Nortershauser, D., and Millan, P., “Inverse Method Using Infrared Thermography for Surface Temperature and Heat Flux Measurements,” *Proceedings of the International Congress on Instrumentation in Aerospace Simulation Facilities*, Vol. 1, 2003, pp. 118–126. <https://doi.org/10.1109/ICIASF.2003.1274861>.
- [22] Nortershauser, D., and Millan, P., “Estimation of moving heat sources with a three-dimensional unsteady inverse method,” *Aerospace Science and Technology*, Vol. 5, No. 8, 2001, pp. 529–540. [https://doi.org/10.1016/S1270-9638\(01\)01130-0](https://doi.org/10.1016/S1270-9638(01)01130-0).
- [23] Klebanoff, P., “Characteristics of turbulence in a boundary layer with zero pressure gradient,” Tech. Rep. NACA Report 1247, NACA, 1954.
- [24] Michel, R., Quémard, C., and Durand, R., *Application d’un schéma de longueur de mélange à l’étude des couches limites turbulentes d’équilibre*, Note technique ONERA No 154, 1969.
- [25] Launder, B., and Shima, N., “Second-moment closure for the near-wall sublayer - Development and application,” *AIAA Journal*, Vol. 27, No. 10, 1989, pp. 1319–1325. <https://doi.org/10.2514/3.10267>.
- [26] Wilcox, D., “Reassessment of the scale-determining equation for advanced turbulence models,” *AIAA Journal*, Vol. 26, No. 11, 1988, pp. 1299–1310. <https://doi.org/10.2514/3.10041>.
- [27] Houdeville, R., “Three-Dimensional Boundary Layer Calculation by a Characteristic Method,” *The 5th Symposium on Numerical and Physical Aspects of Aerodynamical Flows*, Vol. NASA N93-27567, 1992. URL <https://ntrs.nasa.gov/archive/nasa/casi.ntrs.nasa.gov/19930018278.pdf>.
- [28] Arnal, D., “Transition prediction in transonic flow,” *Symposium Transsonicum III*, Springer, 1989, pp. 253–262.
- [29] Bégou, G., Deniau, H., Vermeersch, O., and Casalis, G., “Database approach for laminar-turbulent transition prediction: Navier–Stokes compatible reformulation,” *AIAA Journal*, Vol. 55, No. 11, 2017, pp. 3648–3660. <https://doi.org/10.2514/1.J056018>.
- [30] Mack, L., “Boundary-layer linear stability theory,” Tech. rep., California Inst of Tech Pasadena Jet Propulsion Lab, 1984.
- [31] Dhawan, S., and Narasimha, R., “Some properties of boundary layer flow during the transition from laminar to turbulent motion,” *Journal of Fluid Mechanics*, Vol. 3, No. 4, 1958, pp. 418–436. <https://doi.org/10.1017/S0022112058000094>.

- [32] Stock, H., and Haase, W., “Navier-Stokes airfoil computations with  $e^n$  transition prediction including transitionnal flow regions,” *AIAA Journal*, Vol. 38, No. 11, 2000, pp. 2059–2066. <https://doi.org/10.2514/2.893>.
- [33] Verstraete, T., and Scholl, S., “Stability analysis of partitioned methods for predicting conjugate heat transfer,” *International Journal of Heat and Mass Transfer*, Vol. 101, 2016, pp. 852–869. <https://doi.org/https://doi.org/10.1016/j.ijheatmasstransfer.2016.05.041>.
- [34] Richter, K., Wolf, C., Gardner, A., and Merz, C., “Detection of Unsteady Boundary Layer Transition Using Three Experimental Methods,” 54<sup>th</sup> *AIAA Aerospace Sciences Meeting*, SciTech, San Diego, California, USA, 2016. <https://doi.org/10.2514/6.2016-1072>.
- [35] Rocco Moretti, R., Errera, M., Couaillier, V., and Feyel, F., “Stability, convergence and optimization of interface treatments in weak and strong thermal fluid-structure interaction,” *International Journal of Thermal Sciences*, Vol. 126, 2018, pp. 23–37. <https://doi.org/https://doi.org/10.1016/j.ijthermalsci.2017.12.014>.